



Exact and variational theorems for fracture mechanics of composites with residual stresses, traction-loaded cracks, and imperfect interfaces

JOHN A. NAIRN

Material Science and Engineering, University of Utah, Salt Lake City, Utah 84112, USA
(e-mail: john.nairn@m.cc.utah.edu)

Received 22 January 1999; accepted in revised form 24 February 2000

Abstract. By partitioning the total stresses in a damaged composite into either mechanical and residual stresses or into initial and perturbation stresses, it was possible to derive several exact results for the energy release rate due to crack growth. These general results automatically include the effects of residual stresses, traction-loaded cracks, and imperfect interfaces. The exact energy release rate results were expressed in terms of exact solutions to reduced composite stress analysis problems. By considering the common situation where the initial stresses are known exactly, but the perturbation stresses are only known approximately, it was possible to derive rigorous upper and lower bounds to the energy release rate for crack growth. Some of the new fracture mechanics equations were applied to crack closure calculations, to fiber fracture and interfacial debonding in the fragmentation test, and to microcracking in composite laminates.

1. Introduction

Composite materials, especially composites reinforced with aligned, high-modulus fibers, are often very close to being linear elastic up to failure. For this reason, many composite fracture models for composites have been developed using linear-elastic fracture mechanics [1, 2]. There is microscopy evidence of large amounts of matrix deformation on fracture surfaces [3], but the fact that this deformation does not lead to non-linear, load-deformation curves suggests it is not a major factor in the global energy released during crack growth. The matrix deformation may play a role in *toughness* [3], but it should be possible to calculate the energy release rate due to crack growth by ignoring such deformation and then assuming that cracks propagate when that energy release rate exceeds the fracture toughness of the composite. The required energy release rate can be calculated from a global energy balance using

$$G = -\frac{d\Pi}{dA} = \frac{d(W - U)}{dA} \quad (1)$$

where Π is thermoelastic potential energy, W is external work, U is thermoelastic internal energy, and dA is an increment in total crack area. [4]. The required terms can be calculated using linear thermoelasticity methods.

The goal of this paper is to apply (1) to general composite fracture problems when the composite is assumed to be a linear elastic material. Despite the simplification of linear elasticity, there are several added complexities in heterogeneous composites materials that make fracture mechanics of composite materials more difficult than the corresponding analysis for homogeneous materials. First, because composites are comprised of materials with disparate thermal expansion coefficients, the phases will inevitably be subjected to residual stresses [5]. These residual stresses can contribute to energy release rate and should be part of every composite fracture model [6]. Second, the heterogeneity of composites sometimes causes cracks to divert in directions that would not be observed in homogeneous materials. If such structure-controlled crack growth results in crack surfaces that contact each other, there may be crack surface tractions. When traction-loaded crack surfaces slide relative to each other during crack growth, that sliding can affect the energy release rate. Third, there will always be interfaces between phases. If these interfaces are not perfect, they may slide relative to each other during crack growth [7]. Like sliding traction-loaded cracks, sliding

imperfect interfaces can affect the energy release rate. The main results of this paper are to apply (1) to general composite fracture problems and derive several new and exact results for energy release rate. All new results include the effects of residual stresses, traction-loaded crack surfaces, and imperfect interfaces.

The fracture mechanics results for composites are derived in the section on **Fracture Mechanics Theorems**. The basic method was to partition the total stresses into residual and mechanical stresses or into initial and perturbation stresses. Then, by various applications of virtual work theorems and the divergence theorem it was possible to express (1) in several alternate forms that are more convenient for analysis of particular composite fracture problems. A total-stress form was derived by recombining either of the partitioned-stress results. All new equations are exact but were expressed in terms of exact solutions to composite stress analysis problems that typically will not have exact solutions. A previous paper [6] derived related *exact* expressions but only considered residual and mechanical stress partitioning and traction-free cracks; this paper extends that work to include traction-loaded cracks and imperfect interfaces and to additionally consider initial and perturbation stress partitioning. By partitioning the total stresses into *exact* initial stresses and *approximate* perturbation stresses, it was possible to recast the exact results as rigorous bounds to the energy release rate for crack growth. It is shown how these bounds can be applied to finite fracture mechanics analysis of composite fracture events. A previous paper [8] derived a rigorous upper bound to the finite energy release rate when there are traction-free cracks; this paper extends that work to include both upper and lower bounds, to derive bounds for both infinitesimal and finite fracture events, and to include the effects of traction-loaded cracks and imperfect interfaces. Section 3 shows how the new results can be applied to crack closure calculations, to fiber fracture and interfacial debonding in the fragmentation test, and to microcracking in composite laminates.

2. Fracture Mechanics Theorems

Consider an arbitrary composite subjected to a uniform temperature change of $\Delta T = T$ and to any mixed traction and displacement boundary conditions as illustrated in Fig. 1. Let the boundary be $S = S_T \cup S_u$, where S_T is that part of the surface subjected to traction boundary conditions and S_u is that part of the surface subjected to displacement boundary conditions. Let $\boldsymbol{\sigma}$, with associated tractions on the boundary of $\vec{T} = \boldsymbol{\sigma} \hat{n}$ where \hat{n} is a unit normal to the surface, and $\boldsymbol{\varepsilon}$, with associated displacements \vec{u} , be the exact solution to the linear thermoelasticity problem

$$\begin{aligned} \boldsymbol{\sigma} \hat{n} &= \vec{T}^0 & \text{on} & S_T \\ \vec{u} &= \vec{u}^0 & \text{on} & S_u \\ \boldsymbol{\sigma} &= \mathbf{C}(\boldsymbol{\varepsilon} - \boldsymbol{\alpha}T) & \text{and} & \boldsymbol{\varepsilon} = \mathbf{S}\boldsymbol{\sigma} + \boldsymbol{\alpha}T \end{aligned} \quad (2)$$

where, in addition, $\boldsymbol{\sigma}$ satisfies equilibrium and $\boldsymbol{\varepsilon}$ and \vec{u} satisfy strain-displacement relations. The terms \mathbf{C} , \mathbf{S} , and $\boldsymbol{\alpha}$ are the stiffness, compliance, and thermal expansion tensors; in composites these material properties will depend on position. For arbitrary problems, the traction \vec{T}^0 , and displacement, \vec{u}^0 , boundary conditions may also depend on position. Note also that tractions and displacements may be applied over the same portions of the surface provided they are applied along orthogonal directions.

Let the interior of the composite contain cracks and interfaces and denote the total surface area of cracks and interfaces as S_c . Across any crack or interface, static equilibrium requires that stresses be continuous, but displacements may be discontinuous. When cracks open, the surfaces will be traction free which corresponds to continuous zero stresses. The displacements, however, may be discontinuous as the two surfaces displace independently. When cracks close there may be contact compressive or shear stresses. These stress will be continuous but displacements may be discontinuous as the crack surfaces slide relative to each other. Interfaces may be *perfect* or *imperfect*. At perfect interfaces, stresses and displacement are continuous. Imperfect interfaces can be modeled by requiring continuous stresses, but allowing displacements to be discontinuous [7]. Thus opened cracks, closed cracks, perfect interfaces, and imperfect interfaces can all be included in the single interior surface S_c with continuous stresses but possibly discontinuous displacements. An additional boundary condition on S_c is

$$\vec{T} = \vec{T}_c \quad \text{on} \quad S_c \quad (3)$$

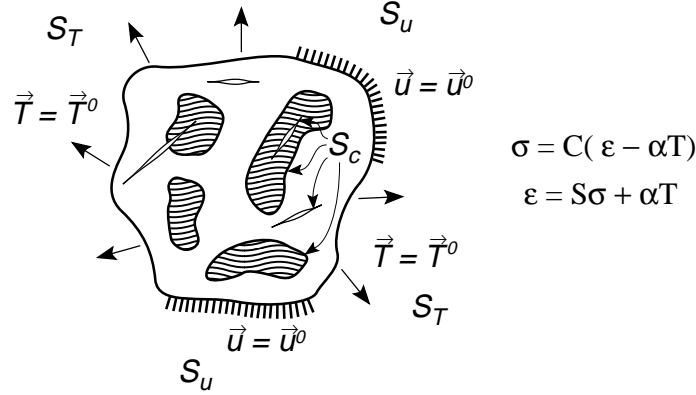


Figure 1. An arbitrary multiphase material subjected to traction and displacement boundary conditions and containing cracks and interfaces.

where \vec{T}_c includes traction loads on any cracks or tractions induced at sliding interfaces. In general, \vec{T}_c may depend on position.

The goal of this section is derive exact and variational theorems for the energy release rate due to an increase in total crack area for the arbitrary composite in Fig. 1. An increase in crack area corresponds to an increase in the internal area S_c .

2.1. MECHANICAL AND RESIDUAL STRESSES

The full thermal elasticity problem can be treated as a superposition of two problems. First, let σ^m and ϵ^m , with tractions \vec{T}^m and displacements \vec{u}^m , be the exact solution to the isothermal ($T = 0$) elasticity problem:

$$\sigma^m \hat{n} = \vec{T}^0 \text{ on } S_T, \quad \vec{u}^m = \vec{u}^0 \text{ on } S_u, \quad \sigma^m = C\epsilon^m, \quad \text{and } \epsilon^m = S\sigma^m \quad (4)$$

Second, let σ^r and ϵ^r , with tractions \vec{T}^r and displacements \vec{u}^r , be the exact solution to the thermal elasticity problem:

$$\sigma^r \hat{n} = 0 \text{ on } S_T, \quad \vec{u}^r = 0 \text{ on } S_u, \quad \sigma^r = C(\epsilon^r - \alpha T), \quad \text{and } \epsilon^r = S\sigma^r + \alpha T \quad (5)$$

A superposition of the above two solutions, $\sigma = \sigma^m + \sigma^r$ and $\epsilon = \epsilon^m + \epsilon^r$, exactly solves the complete thermal elasticity problem in (2) and (3) provided

$$\vec{T}^m + \vec{T}^r = \vec{T}_c \quad \text{on } S_c \quad (6)$$

σ^m and ϵ^m are the mechanical stresses and strains while σ^r and ϵ^r are the residual thermal stresses and strains.

By substituting the partitioned stresses into (1) and making use of virtual work and divergence theorems (the details are in the Appendix), it is possible to derive the first energy release rate theorem:

$$G = G_{mech} + \frac{VT}{2} \left(2 \frac{d \langle \sigma^m \cdot \alpha \rangle}{dA} + \frac{d \langle \sigma^r \cdot \alpha \rangle}{dA} \right) + \frac{d}{dA} \left(\int_{S_c} \vec{T}^r \cdot \vec{u}^m dS + \frac{1}{2} \int_{S_c} \vec{T}^r \cdot \vec{u}^r dS \right) \quad (7)$$

where G_{mech} is the mechanical energy release rate or the energy release when $T = 0$:

$$G_{mech} = \frac{d}{dA} \left(\frac{1}{2} \int_{S_T} \vec{T}^0 \cdot \vec{u}^m dS - \frac{1}{2} \int_{S_u} \vec{T}^m \cdot \vec{u}^0 dS + \frac{1}{2} \int_{S_c} \vec{T}^m \cdot \vec{u}^m dS \right) \quad (8)$$

and angle brackets indicates a volume-averaged quantity:

$$\langle f(x, y, z) \rangle = \frac{1}{V} \int_V f(x, y, z) dV \quad (9)$$

Equation (7) is exact. The first term is the traditional energy release rate. The subsequent terms are required in many composite fracture problems to account for effects of residual stresses, traction-loaded cracks, and imperfect interfaces. A similar analysis for traction-free cracks and perfect interfaces is given in Ref. 6. The new terms above involving integrals over S_c extend those results to include traction-loaded cracks and imperfect interfaces.

In Ref. 6, it was argued that during pure mode I crack growth (or similarly during pure mode II or mode III crack growth) the mode I energy release rate must scale with mode I stress intensity factor squared, K_I^2 . Furthermore, for linear elastic materials in which all applied tractions and displacements are scaled by a factor P and the temperature difference T is scaled by a factor T^* , K_I must scale by a linear combination of P and T^* . Thus

$$G_I \propto K_I^2 = (c_1 P + c_2 T^*)^2 \quad (10)$$

Comparing (10) to (7) similarly scaled by P and T^* , we can prove that

$$\frac{\frac{VT}{2} \frac{d\langle \boldsymbol{\sigma}^m \cdot \boldsymbol{\alpha} \rangle}{dA} + \frac{1}{2} \frac{d}{dA} \int_{S_c} \vec{T}^r \cdot \vec{u}^m dS}{G_{mech}} = \frac{\frac{VT}{2} \frac{d\langle \boldsymbol{\sigma}^r \cdot \boldsymbol{\alpha} \rangle}{dA} + \frac{1}{2} \frac{d}{dA} \int_{S_c} \vec{T}^r \cdot \vec{u}^r dS}{\frac{VT}{2} \frac{d\langle \boldsymbol{\sigma}^m \cdot \boldsymbol{\alpha} \rangle}{dA} + \frac{1}{2} \frac{d}{dA} \int_{S_c} \vec{T}^r \cdot \vec{u}^m dS} \quad (11)$$

Substitution into (7) gives the pure mode I energy release rate of

$$\frac{G_I}{G_{mech}} = \left(1 + \frac{\frac{VT}{2} \frac{d\langle \boldsymbol{\sigma}^m \cdot \boldsymbol{\alpha} \rangle}{dA} + \frac{1}{2} \frac{d}{dA} \int_{S_c} \vec{T}^r \cdot \vec{u}^m dS}{G_{mech}} \right)^2 \quad (12)$$

This result extends the analogous result in Ref. 6 to include traction-loaded cracks and imperfect interfaces.

2.2. TOTAL STRESSES

Sometimes it is simpler to have an energy release rate result in terms of *total* stresses instead of partitioned stresses. By comparing the two virtual work results in the Appendix in (87) and (88) we quickly derive

$$\int_V \boldsymbol{\sigma}^m \cdot \boldsymbol{\alpha} T dV = \int_{S_T} \vec{T}^0 \cdot \vec{u}^r dS - \int_{S_u} \vec{T}^r \cdot \vec{u}^0 dS + \int_{S_c} \vec{T}^m \cdot \vec{u}^r dS - \int_{S_c} \vec{T}^r \cdot \vec{u}^m dS \quad (13)$$

Substituting half of (13) for half of the $\langle \boldsymbol{\sigma}^m \cdot \boldsymbol{\alpha} \rangle$ term in (7) leads to a second energy release rate theorem, now in terms of total stresses ($\boldsymbol{\sigma}$), tractions (\vec{T}), and displacements (\vec{u}):

$$G = \frac{1}{2} \frac{d}{dA} \left(\int_{S_T} \vec{T}^0 \cdot \vec{u} dS - \int_{S_u} \vec{T} \cdot \vec{u}^0 dS + \int_{S_c} \vec{T} \cdot \vec{u} dS + \int_V \boldsymbol{\sigma} \cdot \boldsymbol{\alpha} T dV \right) \quad (14)$$

For the special case of traction-only boundary conditions, (14) followed by use of the divergence theorem leads to

$$G = \frac{1}{2} \frac{d}{dA} \left(\int_{S+S_c} \vec{T}^0 \cdot \vec{u} dS + \int_V \boldsymbol{\sigma} \cdot \boldsymbol{\alpha} T dV \right) = \frac{d}{dA} \int_V \left(\frac{1}{2} \boldsymbol{\sigma} \mathbf{S} \boldsymbol{\sigma} + \boldsymbol{\sigma} \cdot \boldsymbol{\alpha} T \right) dV \quad (15)$$

This result is identical to the thermoelastic fracture mechanics result derived by Hashin [8]. In other words, (14) extends Hashin's analysis (*i.e.* (15)) to include mixed boundary conditions. Note also that the integrand in (15) is minus the Gibb's free energy, F (written as F here to avoid confusion with energy release rate G), less entropy or heat capacity terms [9–11]. Because the constant heat-capacity terms drop out when evaluating the derivative with respect to crack area for an elastic material, (15) shows that energy release rate is equal to a Gibb's free energy derivative, $G = -dF/dA$, when there are traction-only boundary conditions.

2.3. INITIAL AND PERTURBATION STRESSES

To derive some alternative fracture mechanics theorems, including results that help derive a variational fracture mechanics theorem, we consider a different stress partitioning scheme. The full thermal elasticity problem can alternatively be partitioned into *initial* and *perturbation* stresses. First, let σ^0 and ε^0 , with tractions \vec{T}^0 and displacements \vec{u}^0 , be the exact solution to the thermal elasticity problem:

$$\sigma^0 \hat{n} = \vec{T}^0 \text{ on } S_T, \quad \vec{u} = \vec{u}^0 \text{ on } S_u, \quad \sigma^0 = \mathbf{C}(\varepsilon^0 - \alpha T), \quad \text{and } \varepsilon^0 = \mathbf{S}\sigma^0 + \alpha T \quad (16)$$

for any composite which may have cracks and imperfect interfaces on an initial surface S_c^0 . Now let S_c^0 expand into a larger crack and imperfect surface area, S_c , and, let σ^p and ε^p , with tractions \vec{T}^p and displacements \vec{u}^p , be the exact solution to the isothermal ($T = 0$) elasticity problem:

$$\vec{T}^p = 0 \text{ on } S_T, \quad \vec{u}^p = 0 \text{ on } S_u, \quad \vec{T}^p = \vec{T}_c - \vec{T}_c^0 \text{ on } S_c, \quad \sigma^p = \mathbf{C}\varepsilon^p \quad \text{and } \varepsilon^p = \mathbf{S}\sigma^p \quad (17)$$

where \vec{T}_c^0 is the initial stress state traction at the locations of the cracks and interfaces on S_c . Note that \vec{T}^p may be nonzero on S_u and \vec{u}^p may be nonzero on S_T and S_c . A superposition of the above two solutions, $\sigma = \sigma^0 + \sigma^p$ and $\varepsilon = \varepsilon^0 + \varepsilon^p$, exactly solves the complete thermal elasticity problem in (2) and (3). σ^0 and ε^0 are the *initial* stresses and strains; σ^p and ε^p are the *perturbation* stresses and strains or the change in stresses and strains due to growth of traction-loaded cracks and sliding of imperfect interfaces.

By substituting initial and perturbation stresses into (1) and making use of virtual work and divergence theorems (the details are in the Appendix), it is possible to derive a third energy release rate theorem expressed three different ways:

$$\begin{aligned} G &= \frac{d}{dA} \left(\int_{S_c} \vec{T}^p \cdot \vec{u}^0 dS + \frac{1}{2} \int_{S_c} \vec{T}^p \cdot \vec{u}^p dS \right) \\ &= \frac{d}{dA} \left(\int_{S_c} \vec{T}^p \cdot \vec{u}^0 dS + \frac{1}{2} \int_V \sigma^p \mathbf{S} \sigma^p dV \right) = \frac{d}{dA} \left(\int_{S_c} \vec{T}^p \cdot \vec{u}^0 dS + \frac{1}{2} \int_V \varepsilon^p \mathbf{C} \varepsilon^p dV \right) \end{aligned} \quad (18)$$

In many problems it may be convenient to take the initial state as the *undamaged* composite with perfect interfaces and the perturbation stresses as the change in stresses due to introduction of cracks and imperfect interfaces. In an undamaged composite \vec{u}^0 must be continuous across all cracks and interfaces. Because the area S_c has two sides and the traction vector \vec{T}^p changes sign from one side to the other, when \vec{u}^0 is continuous, the first integral in each form of (18) vanishes giving the special case result of

$$G = \frac{d}{dA} \left(\frac{1}{2} \int_{S_c} \vec{T}^p \cdot \vec{u}^p dS \right) = \frac{d}{dA} \left(\frac{1}{2} \int_V \sigma^p \mathbf{S} \sigma^p dV \right) dV = \frac{d}{dA} \left(\frac{1}{2} \int_V \varepsilon^p \mathbf{C} \varepsilon^p dV \right) dV \quad (19)$$

In other words, the total energy release rate including residual stresses, traction-loaded cracks, and imperfect interfaces, can be evaluated by finding the change in perturbation stress energy due to formation of damage. Notice that the perturbation stress analysis is an isothermal ($T = 0$) stress analysis. Thus the effect of thermal stresses on the energy release rate can be evaluated here completely by a thermoelasticity analysis of the *undamaged* composite only; there is never a need to conduct a thermoelasticity analysis of a cracked body.

If we partition the total stresses in (14) into initial and perturbation stresses and delete derivatives of the constant initial stresses, we get

$$G = \frac{1}{2} \frac{d}{dA} \left(\int_{S_T} \vec{T}^0 \cdot \vec{u}^p dS - \int_{S_u} \vec{T}^p \cdot \vec{u}^0 dS + \int_{S_c} \vec{T}_c \cdot \vec{u}^0 dS + \int_{S_c} \vec{T}_c \cdot \vec{u}^p dS + \int_V \sigma^p \cdot \alpha T dV \right) \quad (20)$$

This result appears different than (18), but can be shown to be identical. Equating the two virtual work results between initial and perturbation stresses in the Appendix in (93) and (95), gives

$$\int_V \sigma^p \cdot \alpha T dV = \int_{S_u} \vec{T}^p \cdot \vec{u}^0 dS + \int_{S_c} \vec{T}^p \cdot \vec{u}^0 dS - \int_{S_T} \vec{T}^0 \cdot \vec{u}^p dS - \int_{S_c} \vec{T}_c^0 \cdot \vec{u}^p dS \quad (21)$$

Substitution of (21) into (20) and subtracting zero in the form

$$\frac{1}{2} \frac{d}{dA} \left(\int_{S_c} \vec{T}_c^0 \cdot \vec{u}^0 \right) = 0 \quad (22)$$

leads to a result that is identical to (18).

2.4. GENERALIZED “LEVIN” RELATIONS

In a pioneering composite mechanics paper, Levin considered an undamaged composite with traction loading and perfect interfaces [12]. By partitioning the stresses into mechanical and residual stresses and making use of two applications of virtual work, he derived (in the nomenclature of this paper):

$$\int_V \boldsymbol{\sigma}^m \cdot \boldsymbol{\alpha} T dV = \int_{S_T} \vec{T}^0 \cdot \vec{u}^r dS \quad (23)$$

Levin’s result is a special case of (13); in other words, (13) generalizes Levin’s equation to account for mixed boundary conditions, traction-loaded cracks, and imperfect interfaces. Similarly, (21) was derived by two applications of virtual work between partitioned initial and perturbation stresses; it can therefore be considered as a new, generalized, Levin-type relation. In Ref. 12, Levin derived a powerful application of (23) for determining the effective thermal expansion coefficients of a composite from a solution for the mechanical-only stresses in that composite. Here (13) had an important use in deriving the total stress result in (14) from the partitioned mechanical and residual stress result in (7). Similarly, (21) was needed to show the identity between the total stress result in (14) and the perturbation stress result in (18).

2.5. VARIATIONAL THEOREMS

All results in the previous sections are exact, but they are written in terms of exact solutions to composite stresses and strains. In general, such exact solutions will not be known. In this section, we again partition the stresses into initial and perturbation stresses. We assume that the initial stresses are known exactly. We assume that the perturbation stresses and strains result from the formation of a new finite amount a fracture area, ΔA , and that the perturbation stress state is only known approximately. The goal is to find rigorous upper and lower bounds to the total energy release rate, ΔG , due to the fracture event of forming the finite amount of crack area.

First consider an approximate perturbation solution written in terms of an admissible stress state, $\boldsymbol{\sigma}_a^p$. To be an valid admissible stress state, $\boldsymbol{\sigma}_a^p$ must satisfy equilibrium and tractions associated with $\boldsymbol{\sigma}_a^p$ must give the proper boundary conditions on both S_T and S_c . The thermoelastic complementary energy associated with this approximate stress state is [13]

$$\Gamma_a = \frac{1}{2} \int_V (\boldsymbol{\sigma}^0 + \boldsymbol{\sigma}_a^p) \mathbf{S} (\boldsymbol{\sigma}^0 + \boldsymbol{\sigma}_a^p) dV + \int_V (\boldsymbol{\sigma}^0 + \boldsymbol{\sigma}_a^p) \cdot \boldsymbol{\alpha} T dV - \int_{S_u} (\vec{T}^0 + \vec{T}_a^p) \cdot \vec{u}^0 dS \quad (24)$$

Substituting the virtual work result in the Appendix in (95) (which is valid for any admissible stress state), the approximate complementary energy of the composite reduces to

$$\Gamma_a = \Gamma_0 + \int_{S_c} \vec{T}_a^p \cdot \vec{u}^0 dS + \frac{1}{2} \int_V \boldsymbol{\sigma}_a^p \mathbf{S} \boldsymbol{\sigma}_a^p dV \quad (25)$$

where

$$\Gamma_0 = \frac{1}{2} \int_V \boldsymbol{\sigma}^0 \mathbf{S} \boldsymbol{\sigma}^0 dV + \int_V \boldsymbol{\sigma}^0 \cdot \boldsymbol{\alpha} T dV - \int_{S_u} \vec{T}^0 \cdot \vec{u}^0 dS \quad (26)$$

is the exact complementary energy of the initial stresses. By the principle of minimum complementary energy, this approximate result must be greater than the true complementary energy. Defining the true complementary energy from the exact perturbation stresses, $\boldsymbol{\sigma}^p$, and tractions, \vec{T}^p , we have

$$\Gamma_0 + \int_{S_c} \vec{T}^p \cdot \vec{u}^0 dS + \frac{1}{2} \int_V \boldsymbol{\sigma}^p \mathbf{S} \boldsymbol{\sigma}^p dV \leq \Gamma_0 + \int_{S_c} \vec{T}_a^p \cdot \vec{u}^0 dS + \frac{1}{2} \int_V \boldsymbol{\sigma}_a^p \mathbf{S} \boldsymbol{\sigma}_a^p dV \quad (27)$$

By a discrete evaluation of the derivative in (18) for the formation of finite fracture area ΔA causing the stresses to change from $\boldsymbol{\sigma}^0$ to $\boldsymbol{\sigma}^0 + \boldsymbol{\sigma}^p$ followed by a comparison to (27), the energy release rate for the process is seen to be bounded from above by:

$$\Delta G \leq \frac{1}{\Delta A} \left(\int_{S_c} \vec{T}_a^p \cdot \vec{u}^0 dS + \frac{1}{2} \int_V \boldsymbol{\sigma}_a^p \mathbf{S} \boldsymbol{\sigma}_a^p dV \right) \quad (28)$$

If the initial stresses correspond to an undamaged composite with continuous \vec{u}^0 on S_c , the first term vanishes and the upper bound to ΔG is given simply by the stress energy of any admissible perturbation stress state. Hashin previously considered an undamaged initial state, traction-free crack surfaces, and mechanical-only stresses and derived a result identical to (25) [14] but did not have the S_c integral because of the undamaged initial state. Hashin later added residual stresses and derived an upper bound result equivalent to (28) but again lacking the S_c integral [8]. Although Hashin's two analyses used more restrictive assumptions than used here, both his results are all seen to be correct in general for any undamaged initial state, even when there are mixed boundary conditions, traction-loaded cracks, and imperfect interfaces. The new integral over S_c in (28) extends Hashin's results to the case where the initial stress state is for a damaged composite.

For a lower bound to ΔG , we consider approximate solutions based on admissible strain states, ϵ_a^p , and the approximate change in potential energy. To be a valid admissible strain state, ϵ_a^p must be derived from an assumed displacement field, \vec{u}_a^p , which gives the proper boundary conditions on S_u . If the exact, initial stresses have a potential energy Π_0 , the introduction of new damage will cause the potential energy to decrease by an amount $\Delta\Pi = -\Delta G\Delta A$. For any admissible strain state, the approximate potential energy must be greater than the true potential energy. Thus trivially, an approximate change in potential energy, $\Delta\Pi_a$, provides a lower bound to ΔG :

$$\Delta G \geq -\frac{\Delta\Pi_a}{\Delta A} \quad (29)$$

The only work that remains is to express $\Delta\Pi_a$ in a convenient form using the admissible strain state.

The thermoelastic potential energy associated with an approximate, admissible strain state is not given by (98) in the Appendix because that result used (96) which is not valid for general admissible strain states. All other steps used to derive (98), however, are valid for any admissible strain state. Thus, if we eliminate the final use of (96) and use the crack surface boundary conditions, the approximate thermoelastic potential energy can be written as

$$\Pi_a = \Pi_0 - \int_{S_c} (\vec{T}_c - \vec{T}_c^0) \cdot \vec{u}^0 dS - \int_{S_c} (\vec{T}_c - \vec{T}_c^0) \cdot \vec{u}_a^p dS + \frac{1}{2} \int_V \epsilon_a^p \mathbf{C} \epsilon_a^p dV \quad (30)$$

The lower bound to ΔG becomes

$$\Delta G \geq \frac{1}{\Delta A} \left(\int_{S_c} (\vec{T}_c - \vec{T}_c^0) \cdot \vec{u}^0 dS + \int_{S_c} (\vec{T}_c - \vec{T}_c^0) \cdot \vec{u}_a^p dS - \frac{1}{2} \int_V \epsilon_a^p \mathbf{C} \epsilon_a^p dV \right) \quad (31)$$

Again, the first integral vanishes if the initial strain state corresponds to an undamaged composite with \vec{u}^0 continuous on S_c .

We can define the approximate changes in complementary and potential energy due to any admissible stress or strain states, respectively as

$$\Delta\Gamma_a = \frac{1}{2} \int_V \sigma_a^p \mathbf{S} \sigma_a^p dV + \int_{S_c} \vec{T}_a^p \cdot \vec{u}^0 dS \quad (32)$$

$$\Delta\Pi_a = \frac{1}{2} \int_V \epsilon_a^p \mathbf{C} \epsilon_a^p dV - \int_{S_c} (\vec{T}_c - \vec{T}_c^0) \cdot \vec{u}^0 dS - \int_{S_c} (\vec{T}_c - \vec{T}_c^0) \cdot \vec{u}_a^p dS \quad (33)$$

By (28) and (31), the rigorous bounds on the energy release rate due the formation of a finite amount of fracture area are

$$-\frac{\Delta\Pi_a}{\Delta A} \leq \Delta G \leq \frac{\Delta\Gamma_a}{\Delta A} \quad (34)$$

The most common application of these rigorous bounds to composite energy release rate will probably be for the initiation of damage. It will often be possible to derive exact (or essentially exact) results for the stresses in the undamaged composites. The bounds on energy release rate can then be derived from any approximate solutions for the stresses in the cracked composite. In many composite failure analyses, however, the concern is not just with the initiation of damage, but also with the subsequent propagation of damage. If we introduce fracture area as a variable, the total energy release rate due to a fracture event extending damage area from A_1 to A_2 can be written exactly in terms of energy release rates for forming fracture area A_1 or A_2 from the initial undamaged composite:

$$\Delta G(A_1 \rightarrow A_2) = \frac{A_2 \Delta G(0 \rightarrow A_2) - A_1 \Delta G(0 \rightarrow A_1)}{A_2 - A_1} \quad (35)$$

By making use of the rigorous bounds on ΔG for damage initiation, it is possible to rigorously bound the damage propagation energy release rate by

$$-\frac{\Delta\Pi_a(0 \rightarrow A_2) + \Delta\Gamma_a(0 \rightarrow A_1)}{A_2 - A_1} \leq \Delta G(A_1 \rightarrow A_2) \leq \frac{\Delta\Gamma_a(0 \rightarrow A_2) + \Delta\Pi_a(0 \rightarrow A_1)}{A_2 - A_1} \quad (36)$$

Unless the rigorous bounds for damage initiation (from (34)) are very tight, the rigorous bounds for damage propagation (from (36)) are likely to be far apart. Perhaps the rigorous propagation bounds are too pessimistic. Because the admissible stress or strain states each provide approximate solutions, we could continue and define approximate energy release rates derived from each approximate solution using

$$\Delta G_1(A_1 \rightarrow A_2) = \frac{\Delta\Gamma_a(0 \rightarrow A_2) - \Delta\Gamma_a(0 \rightarrow A_1)}{A_2 - A_1} \quad (37)$$

$$\Delta G_2(A_1 \rightarrow A_2) = -\frac{\Delta\Pi_a(0 \rightarrow A_2) - \Delta\Pi_a(0 \rightarrow A_1)}{A_2 - A_1} \quad (38)$$

$\Delta G_1(A_1 \rightarrow A_2)$ and $\Delta G_2(A_1 \rightarrow A_2)$ will, in general, be much closer to each other than the bounds in (36). Perhaps, therefore, in practice, they will provide tighter, albeit non-rigorous, bounds to $\Delta G(A_1 \rightarrow A_2)$. An example of using such *practical* bounds to analyze composite microcracking will be given in the Section 3.

2.6. FINITE FRACTURE MECHANICS

The previous section dealt with a finite amount of fracture growth — ΔA . Traditional fracture mechanics, however, deals with an infinitesimal amount of crack propagation. Such mathematical results can be derived from finite fracture results by taking the limit as $\Delta A \rightarrow 0$, but that limit may not always be appropriate. Many composite failures do not proceed by infinitesimal crack growth, but rather proceed by discrete fracture events [8]. Two examples are fiber fracture events [15] and matrix microcracking events [2]. Associated with any fracture event is a finite amount of new fracture area, ΔA . One could claim that fracture mechanics can not handle fracture events, or one could propose that the fracture event occurs when the total energy release rate for that fracture event, ΔG , exceeds the material toughness for that event. The method of predicting fracture events based on event energy release rate has been used for many composite failure problems such as edge delamination [16], matrix microcracking [2], fiber breakage and interfacial debonding [17], and cracking of coatings [18–20]. Hashin has recently proposed calling this approach to fracture mechanics *finite fracture mechanics* [8]. The results in the previous section provide variational analysis tools for evaluating energy release rate for fracture events. Two examples in the following section give applications of finite fracture mechanics to predicting composite failure.

3. Examples

The five key energy release rate results are in (7), (14), (18), (34), and (36). Some applications using the mechanical and residual stress partitioning of (7) are given in Ref. 6. An analysis using the total stress form of (14) including a traction-loaded crack is given in Ref. 21. This section will give some examples of partitioning into initial and perturbation stresses and using (18), (34), and (36).

3.1. CRACK CLOSURE IN FINITE ELEMENT ANALYSIS

Consider a small amount of crack growth caused by opening the grid between two elements causing new crack surface area ΔA . The initial stresses are taken to be the stresses before the new crack area forms; the perturbation stresses are the change in stresses caused by the new crack growth or by opening the area between two elements. Evaluation of the derivative in (18) by taking the limit as $\Delta A \rightarrow 0$ results in

$$G = \lim_{\Delta A \rightarrow 0} \frac{1}{\Delta A} \left(\int_{S_c} \vec{T}^p \cdot \vec{u}^0 dS + \frac{1}{2} \int_{S_c} \vec{T}^p \cdot \vec{u}^p dS \right) \quad (39)$$

Notice that these integrals extend over the entire crack and interface surfaces in S_c . Most crack closure methods only consider the work required to close the new crack area and thus only integrate over the area

$S = \Delta A$ local to the crack tip [22]. The result in (39) shows that such crack closure calculations are invalid when there are variable tractions along crack surfaces or slippage at imperfect interfaces. A good example of variable crack surface tractions is friction modeled by having the crack surface shear stress, τ , being related to the crack surface normal stress, σ_n , through a friction law $\tau = \mu\sigma_n$ where μ is the coefficient of friction. When a friction-loaded crack is extended by a finite amount ΔA , σ_n may change along the entire crack surface and thus the crack closure integral must consider all of S_c and not just the new crack area of $S = \Delta A$.

The condition for local crack-tip crack-closure calculations to be valid are that \vec{T}^p must be zero except on the area $S = \Delta A$. These conditions are satisfied when all interfaces are perfect and when all crack surfaces are traction free. Under such conditions, (39) reduces to

$$G = \lim_{\Delta A \rightarrow 0} \frac{1}{2\Delta A} \int_{S=\Delta A} (-\vec{T}_c^0 \cdot \vec{u}^p) dS \quad (40)$$

which reduces to a standard crack closure integral when account is made for integration over both surfaces of the new crack area [22]. Local crack closure is also valid in the presence of crack surface tractions, *provided* there is no change in crack surface tractions along the original crack surfaces. For this situation, \vec{T}^p will be zero every place except on $S = \Delta A$ near the crack tip. Such tractions are included in (40) by replacing $-\vec{T}_c^0$ with $\vec{T}_c - \vec{T}_c^0$ where \vec{T}_c is the constant crack surface traction.

3.2. FRAGMENTATION TEST

In the fragmentation test [15], a single fiber is embedded in a large amount of matrix and the specimen is loaded in tension until the fiber fragments. On continued loading the fiber continues to fragment eventually forming a roughly periodic array of fiber fragments. To analyze a fragmentation specimen, we consider a unit cell of damage or a single fiber fragment as illustrated in Fig. 2. The fiber fragment is of length l and radius r_f ; the matrix is assumed to be infinite. The stresses are partitioned into initial and perturbation stresses. The initial stresses can easily be found by an exact analysis to two concentric cylinders with a perfect interface (Fig. 2B); such a solution is given in Ref. 23. The boundary conditions for *normalized* perturbation stresses are zero displacement on the matrix ends and -1 compression on the fiber ends (Fig. 2C). The full perturbation stresses are obtained by multiplying the normalized result by ψ_∞ where ψ_∞ is the initial axial stress in the fiber and is given in Ref. 23; superscript p in this section indicates *normalized* perturbation stresses and displacements.

We can analyze the fragmentation specimen using (18). The crack and interface surfaces, S_c , include the two fiber breaks and the matrix and fiber surfaces along the interface at $r = r_f$. The fiber fracture surfaces are traction free; thus on the two fiber ends

$$(\vec{T}_c - \vec{T}_c^0) \cdot \psi_\infty \vec{u}^p = \mp \psi_\infty^2 w_f^p(\pm l/2, r) \quad (41)$$

On the fiber/matrix interfacial surfaces:

$$\text{Fiber Surface : } (\vec{T}_c - \vec{T}_c^0) \cdot \psi_\infty \vec{u}^p = \psi_\infty^2 \left[\tau_{rz}^p(z, r_f) w_f^p(z, r_f) + (\sigma_{rr}^p(z, r_f) - \sigma^*) u_f^p(z, r_f) \right] \quad (42)$$

$$\text{Matrix Surface : } (\vec{T}_c - \vec{T}_c^0) \cdot \psi_\infty \vec{u}^p = -\psi_\infty^2 \left[\tau_{rz}^p(z, r_f) w_m^p(z, r_f) + (\sigma_{rr}^p(z, r_f) - \sigma^*) u_m^p(z, r_f) \right] \quad (43)$$

where $w_f^p(z, r)$ and $w_m^p(z, r)$ are the perturbation axial displacements of the fiber and matrix, $u_f^p(z, r)$ and $u_m^p(z, r)$ are the perturbation radial displacements of the fiber and matrix, $\tau_{rz}^p(z, r_f)$ and $\sigma_{rr}^p(z, r_f)$ are the perturbation interfacial stresses, and $\psi_\infty \sigma^*$ is the interfacial radial stress in the initial stresses [23]. Notice that $\tau_{r\theta}^p$ is zero due to axisymmetry and thus there is no term from the hoop displacements. Substitution of the S_c conditions into (18) and assuming symmetry about $z = 0$ gives

$$G = -\pi \psi_\infty^2 \frac{d}{dA} \left[r_f^2 \left\langle w_f^p(l/2) \right\rangle + r_f \int_{-l/2}^{l/2} \tau_{rz}^p(z, r_f) [w^p] dz \right] \quad (44)$$

Here $\left\langle w_f^p(l/2) \right\rangle$ is the *average* axial perturbation displacement on the fiber end and $[w^p] = w_m^p(z, r_f) - w_f^p(z, r_f)$ is the axial displacement discontinuity at the fiber/matrix interface. There is also a term involving

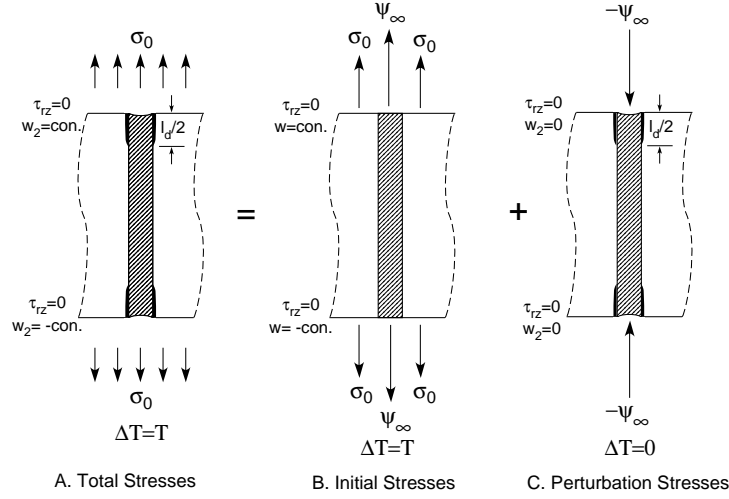


Figure 2. The analysis of a single fiber fragment (A) can be partitioned into the initial stresses (B) and the perturbation stresses (C). The initial stresses are the stresses for an infinitely long, unbroken fiber in an infinite matrix under an applied stress of σ_0 and temperature differential of T . The perturbation stresses are the stresses for a fiber fragment loaded by compression stress of ψ_∞ while the matrix ends are maintained at zero displacement. The notation “con.” means a constant that is independent of r .

radial displacement discontinuity, $[u^p]$, but because the radial stresses are predominantly compressive, it has been argued that the radial displacement discontinuity is zero even in the presence of an imperfect interface [17, 23]; it was assumed to be zero for the derivation of (44).

Two previous papers [17, 23] considered the energetics of the fragmentation specimen. After conversion of the dimensionless results in those papers to the dimensioned results used here, there is found to be a difference between (44) and the previous results. The difference is a change of sign on the second term in (44) or the integral along the interface. The previous papers argued that because of the infinite matrix, there is no external work and G reduces to $G = -dU/dA$. That argument was wrong. When there are traction-loaded cracks or imperfect interfaces, there is the potential for external work along S_c . The general theory in this paper includes all external work and thus (44) corrects the errors in Refs. 17 and 23. Fortunately, the correction only affects the magnitude of some previous results and does not alter any conclusions. Additionally, for the case of perfect interfaces and traction-free cracks, the second term in (44) vanishes and the results in Refs. 17 and 23 are correct.

3.3. FIBER BREAKAGE WITH AN IMPERFECT INTERFACE

Hashin has proposed a simple imperfect interface model where the displacement discontinuity is linearly related to the associated stress at the interface [7] which for the fragmentation test reduces to

$$[w^p] = \frac{\tau_{rz}^p(r_f)}{D_s} \quad (45)$$

where D_s is a property of the interface or interphase. $D_s \rightarrow \infty$ corresponds to a perfect interface; any other D_s describes an imperfect interface with $D_s \rightarrow 0$ corresponding to a traction-free debonded interface. Substitution in (44) and evaluating the discrete derivative for the fiber fragment of length l breaking into two fragments of length $l/2$ with $dA = \pi r_f^2$, the total energy release rate for fiber fracture is

$$\Delta G_f = \psi_\infty^2 (2H(l/2) - H(l)) \quad (46)$$

where after defining a new interface parameter $d_s = r_f D_s$

$$H(l) = -\langle w_f^p(l/2) \rangle - \frac{1}{d_s} \int_{-l/2}^{l/2} (\tau_{rz}^p(r_f))^2 dz \quad (47)$$

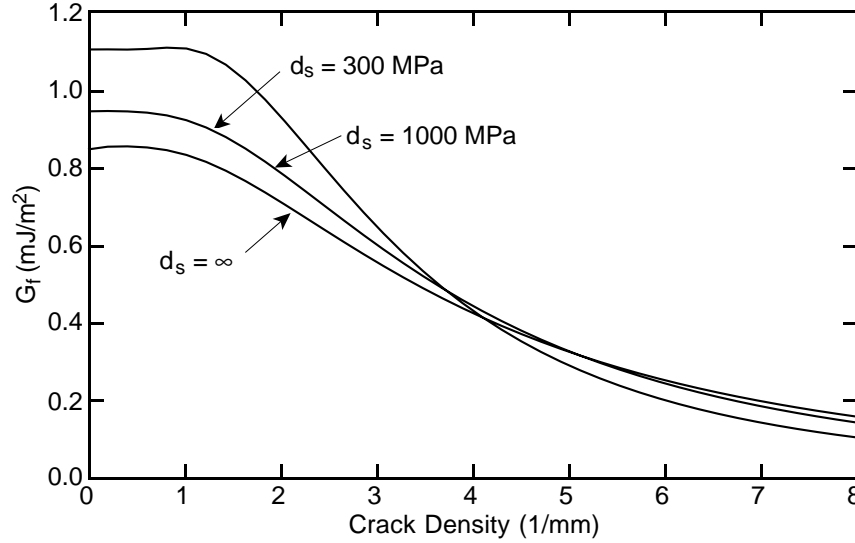


Figure 3. Energy release rate for a fiber fracture event as a function of the crack density of fiber breaks for various values of the interface parameter, d_s . These calculations were for a glass fiber ($E_f = 72$ GPa, $v_f = 0.20$, and $r_f = 7.5 \mu\text{m}$) in a polymeric matrix ($E_m = 1.68$ GPa, $v_m = 0.355$) and an applied axial load adjusted to have $\psi_\infty = 1$.

Sample calculations for ΔG_f as a function of fragment length (1/crack density) for glass fibers in a polymeric matrix and various values of the interface parameter are given in Fig. 3. The required perturbation terms $w_f^p(l/2)$ and $\tau_{rz}^p(r_f)$ for these calculations were found using the Bessel-Fourier stress function analysis derived in Ref. 23. This plot corrects the similar plot in Fig. 2 of Ref. 17 for the sign error in the imperfect interface term in $H(l)$. The corrected sign error causes the changes for a specific d_s vs. $d_s = \infty$ to now be smaller; all trends of the curves, however, are the same and the results with a perfect interface ($d_s = \infty$) are identical. A detailed discussion of ΔG_f is given in Ref. 17. In brief, the energy release rate for the first fiber breaks (at low crack density) gets higher as the interface gets more imperfect. An imperfect interface allows interfacial slip after the fiber break which releases more energy than when slip is prevented by a perfect interface.

3.4. FIBER/MATRIX DEBONDING WITH FRICTION

For a debonding analysis, debond zones of length $l_d/2$ are added to each end of the fragment (see Fig. 2). When there are friction effects, the debonds will be loaded by shear traction. By Coulomb friction, the friction shear-stress should be $\tau_{rz}(z, r_f) = \pm \mu \sigma_{rr}(z, r_f)$ where μ is the coefficient of friction of the fiber/matrix interface and the sign is adjusted depending on the sliding direction. In an exact friction model, one must account for variations in $\sigma_{rr}(z, r_f)$ along the debond; for a simpler model, we assume the friction stresses are constant and given by $\tau_f = \pm \mu \langle \sigma_{rr}(r_f) \rangle$ where $\langle \sigma_{rr}(r_f) \rangle$ is the average interfacial normal stress in the debond zone. The average normal stress must be linearly related to the applied load (ψ_∞). Thus we can write the frictional stresses as $\tau_f = \pm \psi_f \psi_\infty$ where ψ_f is an *effective* coefficient of friction. The correct signs for τ_f are to be negative in the debond zone at $z = -l/2$ and positive in the debond zone at $z = l/2$. Finally, because the above fragmentation analysis used normalized perturbation stresses, the normalized shear stress in the debond zone of this friction model are $\tau_{rz}^p(z, r_f) = \pm \psi_f$.

For simplicity, we assume symmetric debonding damage and a perfect interface in the bonded zone. Generalizations to unsymmetric damage and imperfect interfaces are not difficult. Substitution into (44) then gives

$$G = -\pi r_f^2 \psi_\infty^2 \frac{d}{dA} \left[\left\langle w_f^p(l/2) \right\rangle + \frac{\psi_f l_d}{r_f} \left\langle [w^p(l_d)] \right\rangle \right] \quad (48)$$

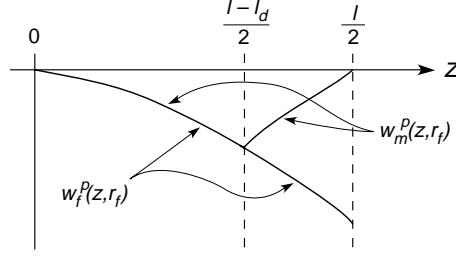


Figure 4. The expected form of the interfacial axial displacement in the fiber and matrix for the perturbation stress analysis of a single fiber fragment and $z > 0$. Note that the fiber and matrix interfacial displacements are equal in the central intact zone, but are discontinuous in the debond zone.

where $\langle [w^p(l_d)] \rangle$ is the average axial displacement discontinuity along the debond:

$$\langle [w^p(l_d)] \rangle = \frac{2}{l_d} \int_{(l-l_d)/2}^{l/2} [w^p] dz \quad (49)$$

This result is exact for debonds with a constant friction stress. Next we consider some accurate assumptions without actually undertaking stress analysis of the fragmentation specimen.

The exact result depends on $\langle [w^p(l_d)] \rangle$ which requires a 3D axisymmetric analysis and accurate evaluation of the fiber and matrix displacements at the interface. A schematic view of the exact displacements for $z > 0$ is given in Fig. 4. To approximate the displacement discontinuity in the debond zone, we assume the fiber interfacial displacement is approximately equal to the *average* axial fiber displacement and we write the matrix axial displacement as a monotonic extrapolation between its boundary condition at $l/2$ ($w_m^p(l/2, r_f) = 0$) and its continuity condition at the debond tip ($w_m^p((l-l_d)/2, r_f) = w_f^p((l-l_d)/2, r_f)$). The interfacial displacements then become

$$w_f^p(z, r_f) \approx \langle w_f^p(z) \rangle \quad \text{and} \quad w_m^p(z, r_f) = m(z) w_f^p((l-l_d)/2, r_f) \approx m(z) \langle w_f^p((l-l_d)/2) \rangle \quad (50)$$

where the matrix extrapolation function, $m(z)$, monotonically increases from $m(l/2) = 0$ to $m((l-l_d)/2) = 1$. Substitution into (48) leads to

$$G = \pi r_f^2 \psi_\infty^2 \frac{d}{dA} \left\{ -F(l/2) + \frac{2\psi_f}{r_f} \int_{(l-l_d)/2}^{l/2} F(z) dz - \left(1 - \frac{M\psi_f l_d}{r_f} \right) \langle w_f^p((l-l_d)/2) \rangle \right\} \quad (51)$$

where

$$M = 1 - \frac{2}{l_d} \int_{(l-l_d)/2}^{l/2} m(z) dz \quad \text{and} \quad F(z) = \langle w_f^p(z) \rangle - \langle w_f^p((l-l_d)/2) \rangle = \int_{(l-l_d)/2}^z \langle \varepsilon_{zz,f}^p(z) \rangle dz \quad (52)$$

The constant M depends on the selected extrapolation function but it must be between 0 and 1. Here M will be assumed to be in the middle or $M = 1/2$; this assumption corresponds to a linear extrapolation of the matrix displacement.

The function $F(z)$ only depends on the average axial fiber displacements in the debond zone. By an exact equilibrium analysis, the average axial fiber stress in the debond zone must satisfy

$$\frac{d \langle \sigma_{zz,f}^p(z) \rangle}{dz} = -\frac{2\tau_{rz}^p(z, r_f)}{r_f} = -\frac{2\psi_f}{r_f} \quad (53)$$

Integration with boundary condition $\langle \sigma_{zz,f}^p(l/2) \rangle = -1$ gives

$$\langle \sigma_{zz,f}^p(z) \rangle = \frac{2\psi_f}{r_f} \left(\frac{l}{2} - z \right) - 1 \quad (54)$$

If the constant interfacial shear stress is due to friction, then the perturbation axial fiber stress must remain negative in the debond zone otherwise the stress transferred into the fiber would exceed the far-field fiber stress. From this requirement and (54), the analysis in this section is limited to friction or debond lengths sufficiently low that $\psi_\infty l_d/r_f < 1$. We next assume that the average axial displacement in the fiber can be calculated from the axial stress alone; in other words, we ignore transverse stresses and assume

$$\langle \epsilon_{zz,f}^p \rangle = \frac{\langle \sigma_{zz,f}^p \rangle}{E_A} - \frac{\nu_A \langle \sigma_{rr,f}^p \rangle}{E_A} - \frac{\nu_A \langle \sigma_{\theta\theta,f}^p \rangle}{E_A} \approx \frac{\langle \sigma_{zz,f}^p \rangle}{E_A} \quad (55)$$

where E_A and ν_A are the axial modulus and Poisson's ratio of the fiber.

Substituting the debond zone strain into the definition for $F(z)$ and substituting the result into (51) together with $M = 1/2$ leads to the final approximate result:

$$G = \pi r_f^2 \psi_\infty^2 \frac{d}{dA} \left[\frac{l_d}{2E_A} \left(1 - \frac{\psi_f l_d}{r_f} + \frac{\psi_f^2 l_d^2}{3r_f^2} \right) - \left(1 - \frac{\psi_f l_d}{2r_f} \right) \langle w_f^p((l-l_d)/2) \rangle \right] \quad (56)$$

To reiterate, the only approximations used to derive the constant friction stress result in (56) are that the interfacial axial fiber displacement is approximately equal to the average axial fiber displacement, that the matrix axial interfacial displacement varies linearly with z , and that transverse stresses can be ignored when calculating the debond zone axial strain. All these assumptions were checked by some sample finite element calculations and they all appear to be excellent assumptions. We claim, therefore, that (56) is a very accurate result. It has reduced the complete analysis of the fiber fracture and debonding problem to the determination of the average axial fiber displacement at the debond tip $\langle w_f^p((l-l_d)/2) \rangle$.

One could continue and substitute analytical results for $\langle w_f^p((l-l_d)/2) \rangle$ and quickly derive energy release rates for various failure modes involving fiber breakage and friction-loaded debonding. Additional progress can be made, still without any specific stress analysis, by considering the limiting case as $l \rightarrow \infty$; this limit corresponds to non-interacting fiber breaks or fragmentation results at low crack density. In the limit $l \rightarrow \infty$, all perturbation displacements become independent of l and only depend on distance from the fiber break. Furthermore, $\lim_{l \rightarrow \infty} \langle w_f^p((l-l_d)/2) \rangle$, or the displacement at the tip of a long intact zone, is the equal to the displacement at the end of a long fiber with no debonds, but scaled by the amount of stress transferred to the end of the intact zone through the debond zone. From the stress at the debond tip in (54), we can write

$$\lim_{l \rightarrow \infty} \langle w_f^p((l-l_d)/2) \rangle = \left(1 - \frac{\psi_f l_d}{r_f} \right) \lim_{l \rightarrow \infty} \langle w_f^p(l/2) \rangle \quad (57)$$

where $\langle w_f^p(l/2) \rangle$ is evaluated for a fiber with no debonds. Taking the limit of (46) gives

$$\Delta G_{f\infty} = \lim_{l \rightarrow \infty} \Delta G_f = \psi_\infty^2 \lim_{l \rightarrow \infty} \left[\langle w_f^p(l/2) \rangle - 2 \langle w_f^p(l/4) \rangle \right] = -\psi_\infty^2 \lim_{l \rightarrow \infty} \langle w_f^p(l/2) \rangle \quad (58)$$

where subscript ∞ on any G implies the limit of long fragment lengths. Substituting (57) and (58) into (56) gives

$$G_\infty = \pi r_f^2 \psi_\infty^2 \frac{d}{dA} \left[\frac{l_d}{2E_A} \left(1 - \frac{\psi_f l_d}{r_f} + \frac{\psi_f^2 l_d^2}{3r_f^2} \right) + \left(1 - \frac{\psi_f l_d}{2r_f} \right) \left(1 - \frac{\psi_f l_d}{r_f} \right) \frac{\Delta G_{f\infty}}{\psi_\infty^2} \right] \quad (59)$$

If the total debond length surrounding the isolated fiber breaks grows by an amount dl_d , then $dA = 2\pi r_f dl_d$ and the energy release rate for debond growth from an isolated fiber break in the presence of friction is

$$G_{d\infty} = \frac{r_f \psi_\infty^2}{4E_A} \left(1 - \frac{\psi_f l_d}{r_f} \right)^2 - \frac{\psi_f \Delta G_{f\infty}}{4} \left(3 - \frac{2\psi_f l_d}{r_f} \right) \quad (60)$$

In the absence of friction $\psi_f \rightarrow 0$, $G_{d\infty}$ reduces to the Outwater and Murphy [24] result of $G_{d\infty} = r_f \psi_\infty^2 / (4E_A)$. For debonding from isolated fiber breaks, the entire problem has been reduced to finding $\Delta G_{f\infty}$. A Bessel-Fourier stress function result for $\Delta G_{f\infty}$ is shown in Fig. 3 by taking the limiting value

of the $d_s = \infty$ curve at low crack density. A recent examination of the Bessel-Fourier analysis in Ref. 23 suggests it may not be accurate for $\Delta G_{f\infty}$. A refined Bessel-Fourier analysis [17, 25] or refined elasticity models [26] can give improved results. $\Delta G_{f\infty}$ could alternatively be calculated using finite element analysis, but even that method has numerical difficulties dealing with infinitely long fibers in an infinite matrix and with handling the boundary conditions of a cracked fiber with a high modulus embedded in a matrix with a low modulus. Because evaluation of $\Delta G_{f\infty}$ also solves the problem of finding $G_{d\infty}$, it can be claimed as a fundamental problem in analysis of composite failure. Additional theoretical work is required before $\Delta G_{f\infty}$ can be calculated with confidence.

3.5. FINITE FRACTURE MECHANICS OF FIBER FRACTURE AND DEBONDING

Experimental observations on fragmentation specimens for which debonds can be observed by microscopy indicates that fiber breaks are usually accompanied by a certain amount of instantaneous debonding [27–29]. Thus, the fundamental fracture event in the fragmentation test is a fiber break with *simultaneous* debonding of length l_d (or length $l_d/2$ on either side of the fiber break). A finite fracture mechanics analysis of simultaneous fiber breakage and debonding can be derived by asserting that fiber breaks and debonds occur when the total energy released is equal to the total energy required. Using the long-fragment limit results in the previous section, the energy balance becomes

$$\pi r_f^2 \Delta G_{f\infty} + \int_0^{l_d} 2\pi r_f G_{d\infty}(x) dx = \pi r_f^2 \Gamma_f + 2\pi r_f l_d \Gamma_d \quad (61)$$

The left side is the energy released by the fiber fracture and debonding fracture event; the right side is the energy required for the event where Γ_f is the fiber fracture toughness and Γ_d is the debonding fracture toughness. Substituting into (60) and solving for Γ_d leads to

$$\Gamma_d = \frac{r_f \psi_\infty^2}{4E_A} \left(1 - \frac{\psi_f l_d}{r_f} + \frac{\psi_f^2 l_d^2}{3r_f^2} \right) + \frac{r_f \Delta G_{f\infty}}{2l_d} \left(1 - \frac{\psi_f l_d}{2r_f} \right) \left(1 - \frac{\psi_f l_d}{r_f} \right) - \frac{\Gamma_f r_f}{2l_d} \quad (62)$$

Equation (62) can be used to analyze fragmentation experiments and deduce an interfacial fracture toughness [29]. The key experiment is to measure instantaneous debond length at a fiber break as a function of the strain (or equivalently ψ_∞) at which the fiber break occurred [27–29]. With known values of ψ_f and Γ_f and some theory for $\Delta G_{f\infty}$, such experimental results can be used to calculate Γ_d from each data point. Alternatively, substituting (58) and solving for ψ_∞^2 gives:

$$\psi_\infty^2 = \frac{\frac{2l_d \Gamma_d}{r_f} + \Gamma_f}{\frac{l_d}{2E_A} \left(1 - \frac{\psi_f l_d}{r_f} + \frac{\psi_f^2 l_d^2}{3r_f^2} \right) - \lim_{l \rightarrow \infty} \langle w_f^p(l/2) \rangle \left(1 - \frac{\psi_f l_d}{2r_f} \right) \left(1 - \frac{\psi_f l_d}{r_f} \right)} \quad (63)$$

This prediction for applied stress (ψ_∞) as a function of debond length (l_d) can be fit to experimental results to determine Γ_d . Some example predictions are given in Fig. 5 for two values of interfacial toughness and three values of the *effective* friction coefficient. The predicted debond growth increases monotonically with applied strain. Recall, however, that these predictions assume isolated fiber breaks. When the fiber breaks begin to interact, the amount of debond growth will peak and then decrease at higher strain [17, 30]. The prediction curves shift to the right if either the friction or the interfacial toughness increases. When analyzing experimental data without any knowledge of friction, it will not be possible to tell whether the data should be fit with high friction and low toughness or with low friction and high toughness. In other words, the only way to get the correct result for Γ_d is to have independent results to determine the level of friction stresses. With no knowledge of friction, the best fit Γ_d will decrease as the assumed ψ_f increases. An analysis that ignores friction will thus give an upper bound to the *true* interfacial toughness [17]. Some comparisons between debonding experiments and the above type of finite fracture mechanics model are given in Refs. 27–29; these papers either ignored friction [27, 28] or included friction [29]; each calculated $\Delta G_{f\infty}$ using the shear-lag analysis result of $\lim_{l \rightarrow \infty} \langle w_f^p(l/2) \rangle = -r_f/(\beta E_A)$ where β is the dimensionless shear-lag parameter [30, 31].

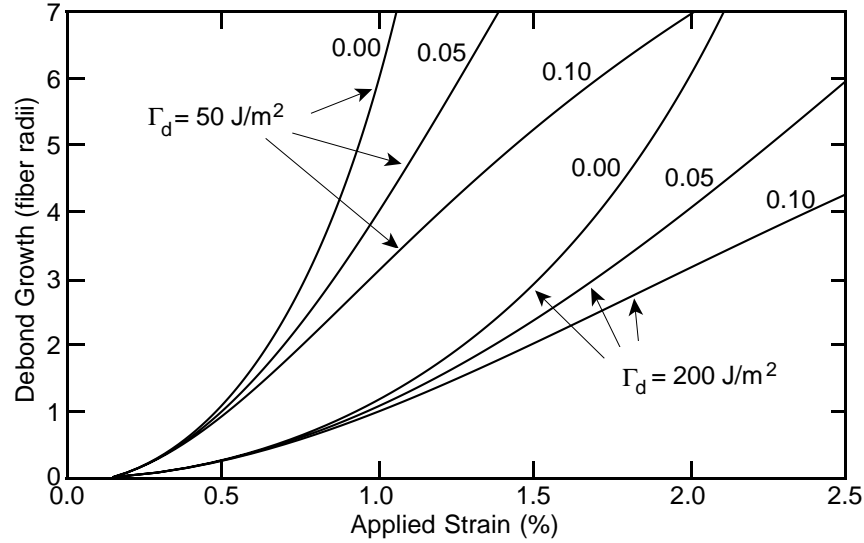


Figure 5. Finite fracture mechanics prediction for the extent of debonding near isolated fiber breaks as a function of the strain required to break the fiber. The interfacial toughness was assumed to be either $\Gamma_d = 200 \text{ J/m}^2$ or 50 J/m^2 ; for each toughness, the friction was set to $\psi_f = 0.0, 0.05$, or 0.1 . The fiber and matrix properties are given in the caption to Fig. 3. The fiber toughness was assumed to be $\Gamma_f = 10 \text{ J/m}^2$. The $\Delta G_{f\infty}$ was found using the Bessel-Fourier analysis of Fig. 3.

3.6. LAMINATE MICROCRACKING

When cross-ply laminates $([0_n/90_m]_s)$ are loaded in tension parallel to the 0° plies, the 90° plies develop transverse cracks or matrix microcracks (see review article Ref. 2). On continued loading, the 90° plies crack into a roughly periodic array of microcracks. For analysis of a microcracked specimen, we consider a unit cell of damage or a single microcrack as illustrated in Fig. 6. Previous work has derived approximate 2D, plane-stress solutions to the stresses in the $x - z$ plane of a microcracked laminate based either on an admissible stress state [14, 32, 33] or an admissible strain state [34]. In this section, these previous solutions will be outlined and modified slightly to be more consistent about boundary conditions and to use the methods in this paper. The slightly modified results will then be used to discuss upper and lower bounds to the finite energy release rate due to formation of microcracks.

3.6.1. Upper bound energy release rate

To derive an upper bound energy release rate solution we consider an approximate solution based on an admissible stress state. For a constant applied axial strain of ε_0 and a plane-stress analysis in the $x - z$ plane, the initial thermoelastic stresses are easily seen to be

$$\begin{aligned} \sigma_{xx,1}^0 &= E_{xx}^{(1)}(\varepsilon_0 - \alpha_{xx}^{(1)}T) & \tau_{xz,1}^0 &= 0 & \sigma_{zz,1}^0 &= 0 \\ \sigma_{xx,2}^0 &= E_{xx}^{(2)}(\varepsilon_0 - \alpha_{xx}^{(2)}T) & \tau_{xz,2}^0 &= 0 & \sigma_{zz,2}^0 &= 0 \end{aligned} \quad (64)$$

where the subscript 1 or 2 on the stresses and superscripts (1) or (2) on the thermomechanical properties indicate terms for the 90° and 0° plies, respectively. Following Hashin [14], perturbation stresses were derived by using one assumption that the axial stresses in each ply group are independent of the z coordinate. From the equations of stress equilibrium, the resulting perturbation stresses become

$$\begin{aligned} \sigma_{xx,1}^p &= -\psi(x) & \tau_{xz,1}^p &= z\psi'(x) & \sigma_{zz,1}^p &= \frac{1}{2}(ht_1 - z^2)\psi''(x) \\ \sigma_{xx,2}^p &= \frac{\psi(x)}{\lambda} + \sigma_{ex} & \tau_{xz,2}^p &= (h - z)\frac{\psi'(x)}{\lambda} & \sigma_{zz,2}^p &= \frac{1}{2}(h - z)^2\frac{\psi''(x)}{\lambda} \end{aligned} \quad (65)$$

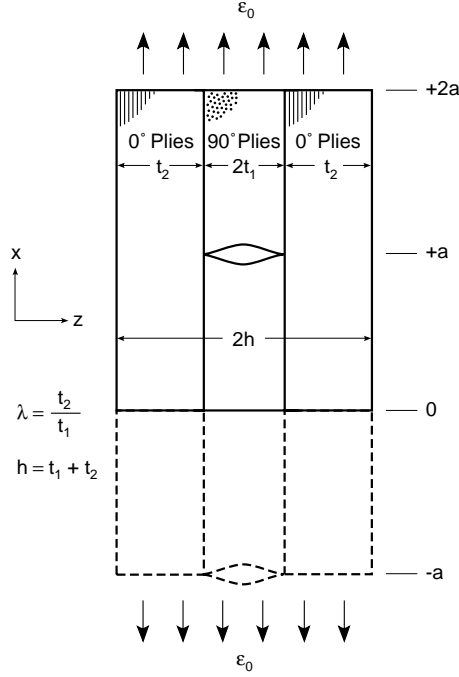


Figure 6. A unit cell of damage for a $[0_n/90_m]_s$ laminate with a periodic array of microcracks spaced by distance $2a$. This figure is an edge view or x - z plane view. The laminate width direction is in the y direction. The axial load is applied in the x direction.

where $\psi(x)$ is an unknown function of x and h , t_1 , and λ are defined in Fig. 6. These perturbation stresses are identical to Hashin [14] except for the addition of σ_{ex} in $\sigma_{xx,2}^p$. Hashin considered traction boundary conditions for which the total axial perturbation stress ($t_1\sigma_{xx,1}^p + t_2\sigma_{xx,2}^p$) must be zero. Here, the analysis is modified to consider displacement boundary conditions; the term σ_{ex} is the excess perturbation stress that appears in the 0° plies after formation of the microcrack. The net perturbation axial stress is now a constant ($t_1\sigma_{xx,1}^p + t_2\sigma_{xx,2}^p = t_2\sigma_{ex}$) instead of zero as in the traction loading analysis.

The unknown function $\psi(x)$ can be found by minimizing the stress energy associated with the perturbation stresses which is equivalent to minimizing the total complementary energy (see (25)). The analysis procedure is identical to the one in Ref. 14. When the solution of $\psi(x)$ is substituted back into the perturbation stress energy, the total complementary energy for the microcrack unit cell reduces to

$$\Gamma_a = \Gamma_0 + Wt_1^2 \left[\frac{2\rho\lambda}{C_1 E_{xx}^{(1)} E_{xx}^{(2)}} \sigma_{ex}^2 + 2C_3 \chi_L(\rho) \left((\sigma_{xx,1}^0)^2 + \frac{\sigma_{ex}}{C_1 E_{xx}^{(2)}} \right)^2 \right] \quad (66)$$

where W is laminate width in the y direction, $\rho = a/t_1$ is the axial ratio of the microcracking interval, $\chi_L(\rho)$ is an excess energy function (defined first by Hashin [14] and later in Ref. 32 for all possible values of laminate properties), C_3 is a constant that depends on laminate properties (see Ref. 35), and

$$C_1 = \frac{(1+\lambda)E_0}{\lambda E_{xx}^{(1)} E_{xx}^{(2)}} \quad (67)$$

where $E_0 = (t_1 E_{xx}^{(1)} + t_2 E_{xx}^{(2)})/h$ is the rule-of mixtures modulus of the laminate. Equation (66) is identical to Hashin's [14] result except for the new term involving σ_{ex} . Minimizing Γ_a with respect to σ_{ex} , the final approximate complementary energy for displacement boundary conditions becomes

$$\Gamma_a = \Gamma_0 + \frac{2Wt_1^2 C_3 (\sigma_{xx,1}^0)^2 \chi_L(\rho)}{1 + \frac{E_{xx}^{(1)}}{E_0} \frac{C_3}{1+\lambda} \frac{\chi_L(\rho)}{\rho}} \quad (68)$$

If the *exact* complementary energy is written in terms of the *exact*, effective axial modulus of a cracked composite with n microcrack intervals of possibly variable aspect ratios, ρ_i , the total complementary energy in the absence of residual stresses ($\sigma_{xx,1}^0 = E_{xx}^{(1)} \varepsilon_0$) can be written as

$$\Gamma = -\frac{1}{2} E_A^* \varepsilon_0^2 \sum_{i=1}^n 4Wt_1^2 (1 + \lambda) \rho_i \quad (69)$$

Combining this result with $\Gamma \leq \Gamma_a$, the definition of C_1 , and

$$\Gamma_0 = -\frac{1}{2} E_0 \varepsilon_0^2 \sum_{i=1}^n 4Wt_1^2 (1 + \lambda) \rho_i \quad (70)$$

we can derive a lower bound to the effective axial modulus of

$$E_A^* \geq \frac{\langle \rho E_A^L(\rho) \rangle}{\langle \rho \rangle} \quad \text{where} \quad \frac{E_0}{E_A^L(\rho)} = 1 + \frac{E_{xx}^{(1)2}}{E_0} \frac{C_3}{1 + \lambda} \frac{\chi_L(\rho)}{\rho} \quad (71)$$

and $\langle \cdot \rangle$ is an average over the n microcrack intervals. Here $E_A^L(\rho)$ is defined as the lower bound modulus for a laminate with exactly periodic microcrack intervals of aspect ratio ρ . In contrast, Hashin's lower bound modulus [14] can be expressed

$$E_A^* \geq \frac{\langle \rho \rangle}{\langle \rho / E_A^L(\rho) \rangle} \quad (72)$$

These two lower bounds are the same for periodic cracks, but differ for variably spaced microcracks. The difference arises from the current constant strain analysis *vs.* Hashin's constant stress analysis.

Substituting (71) into (68) the total change in complementary energy associated with n microcracks of possibly variable aspect ratios, ρ_i , is

$$\Delta \Gamma_a(0 \rightarrow n) = 2Wt_1^2 (\sigma_{xx,1}^0)^2 \left(C_3 \sum_{i=1}^n \frac{E_A^L(\rho_i)}{E_0} \chi_L(\rho_i) \right) \quad (73)$$

The total fracture area associated with n microcracks is $A = 2nt_1W$. Thus, a rigorous upper bound for the energy release rate due to the formation of n microcracks is

$$\Delta G_m(0 \rightarrow n) \leq \frac{\Delta \Gamma_a(0 \rightarrow n)}{2nt_1W} = t_1 (\sigma_{xx,1}^0)^2 \left\langle C_3 \frac{E_A^L(\rho)}{E_0} \chi_L(\rho) \right\rangle \quad (74)$$

For evaluation of the *practical* energy release rate bounds for formation of a single microcrack in the middle of an existing microcrack interval of aspect ratio ρ , substitution into (37) leads to

$$\Delta G_{m1}(n \rightarrow n+1) = C_3 t_1 (\sigma_{xx,1}^0)^2 \left(2 \frac{E_A^L(\rho/2)}{E_0} \chi_L(\rho/2) - \frac{E_A^L(\rho)}{E_0} \chi_L(\rho) \right) \quad (75)$$

This result is similar to previous energy release rate results derived using assumed stress states [2, 32, 35]. It differs, however, in the new factors of $E_A^L(\rho)/E_0$. Although such factors are always less than one, this new energy release rate is not an improved upper bound to energy release. Instead, these factors are a consequence of now analyzing fixed-displacement boundary conditions while all previous analyses were for fixed-load boundary conditions. In fracture mechanics with an infinitesimal amount of crack growth, the final energy release rate is independent of whether the analysis was done for fixed-displacement or fixed-load boundary conditions. For finite fracture mechanics analyses, however, the energy release rate depends on boundary conditions. The dependence illustrated in Fig. 7 which plots loading and unloading load-displacement curves for a finite amount of fracture growth. The total energy released is the area between the loading and unloading curves [4]. For fixed-load boundary conditions, the total energy released is equal to the area of the *ABC* triangle; for fixed-displacement boundary conditions, the total energy released is lower and equal to the shaded area of the *ABD* triangle. Deriving the slopes of the initial loading curve from E_0

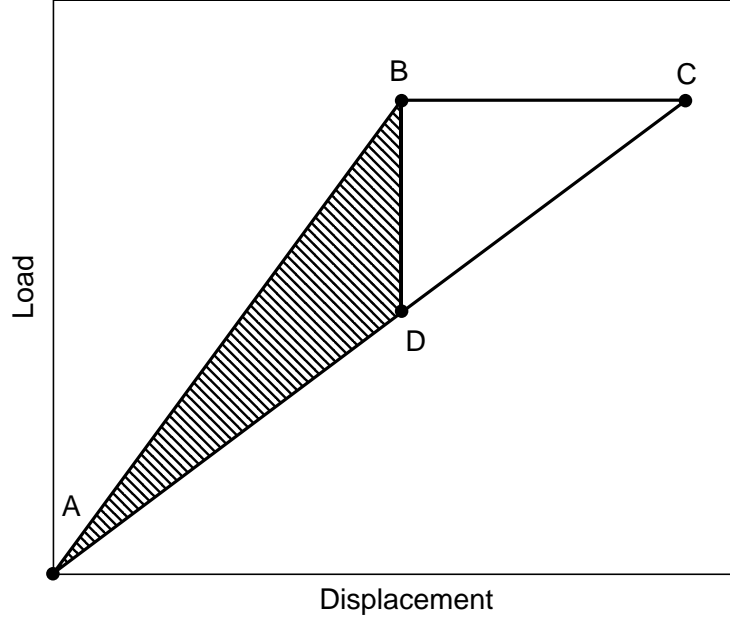


Figure 7. Load-displacement curve for a finite increase in crack area. The area of the ABC triangle is the total energy released by crack growth under load control. The shaded area of the ABD triangle is the total energy released by crack growth under displacement control.

and of the unloading curve from E_A^* , it is easy to show the the ratio of the ABD to ABC triangular areas is E_A^*/E_0 . Thus, the new factors of $E_A^L(\rho)/E_0$ are simply a consequence of now analyzing fixed-displacement boundary conditions. When analyzing real experiments using finite fracture mechanics, it is important to use the correct result for the specific experimental conditions. Most laminate experiments are done using displacement-control experiments and thus the new results derived here are the appropriate ones for finite fracture mechanics analysis of microcracking.

3.6.2. Lower bound energy release rate

To derive an lower bound energy release rate solution we consider an approximate solution based on an admissible strain state. For a constant applied axial strain of ε_0 and a plane-stress analysis in the $x - z$ plane, the initial displacements are easily seen to be

$$\begin{aligned} u_1^0 &= \varepsilon_0 x & w_1^0 &= -\varepsilon_0 \nu_{xz}^{(1)} z \\ u_2^0 &= \varepsilon_0 x & w_2^0 &= -\varepsilon_0 (\nu_{xz}^{(1)} t_1 + \nu_{xz}^{(2)} \varepsilon_0 (z - t_1)) \end{aligned} \quad (76)$$

where u and w are x and z direction displacements, respectively. Following Ref. 34, the perturbation displacements are assumed to be

$$\begin{aligned} u_1^p &= t_1 \psi_1(x) \phi(z) + a_1 x & w_1^p &= z t_1 \psi_2(x) \\ u_2^p &= t_1 \psi_1(x) + a_1 x & w_2^p &= t_1 \psi_2(x) + a_2 (z - t_1) \end{aligned} \quad (77)$$

where $\psi_1(x)$ and $\psi_2(x)$ are two unknown functions of x , $\phi(z)$ is an unknown function of z that describes the crack opening displacement, and a_1 and a_2 are unknown constants. The boundary conditions on $\psi_1(x)$, $\psi_2(x)$, and $\phi(z)$ are $\psi_1(\pm a) = \mp a_1 \rho$, $\psi_2(\pm a) = a_3$ where a_3 is another unknown constant, $\phi(t_1) = 1$, and $\phi'(0) = 0$ [34].

With a given $\phi(z)$, it is possible to minimize the total potential energy to find $\psi_1(x)$, $\psi_2(x)$, a_1 , a_2 , and a_3 . Although Ref. 34 analyzed total displacements and strains and minimized total thermoelastic potential energy, the methods in Ref. 34 can also be used to minimize $\Delta \Pi_a = \Pi_a - \Pi_0$ (see (30)). The final result for

total thermoelastic potential energy is identical to Ref. 34 but the analysis is simpler because it can ignore thermal stress terms, *i.e.*, the perturbation stresses and strains have $T = 0$. The total potential energy can be written as

$$\Pi_a = \Pi_0 - 2Wt_1^2 (\sigma_{xx,1}^0)^2 \frac{\chi_\varepsilon(\rho)}{E_0} \quad (78)$$

where $\chi_\varepsilon(\rho)$ is an energy function defined in Ref. 34 and denoted there as $\chi_U(\rho)$. If we define the *exact* potential energy in terms of the *exact*, effective axial modulus of a cracked composite with n microcrack intervals of possibly variable aspect ratios, ρ_i , the total potential energy in the absence of residual stresses ($\sigma_{xx,1}^0 = E_{xx}^{(1)} \varepsilon_0$) can be written as

$$\Pi = \frac{1}{2} E_A^* \varepsilon_0^2 \sum_{i=1}^n 4Wt_1^2 (1 + \lambda) \rho \quad (79)$$

Combining this result with $\Pi \leq \Pi_a$ and

$$\Pi_0 = \frac{1}{2} E_0 \varepsilon_0^2 \sum_{i=1}^n 4Wt_1^2 (1 + \lambda) \rho \quad (80)$$

we can derive an upper bound to the effective axial modulus of

$$E_A^* \leq \frac{\langle \rho E_A^U(\rho) \rangle}{\langle \rho \rangle} \quad \text{where} \quad \frac{E_0}{E_A^U(\rho)} = 1 + \frac{E_{xx}^{(1)2}}{E_0} \frac{C_3}{1 + \lambda} \frac{\chi_U(\rho)}{\rho} \quad (81)$$

and $\chi_U(\rho) = \chi_\varepsilon(\rho)/(C_3 E_A^U(\rho))$ has been to defined for better comparison between the upper and lower bound results. Here $E_A^U(\rho)$ is defined as the upper bound modulus for a laminate with exactly periodic microcrack intervals of aspect ratio ρ . This upper bound modulus is identical to the upper bound in Ref. 34 (but note that $\chi_U(\rho)$ in Ref. 34 is $\chi_\varepsilon(\rho)$ here).

Combining (78) with (74) and substituting into (34) the rigorous bounds to the energy release rate due to formation of n microcracks are

$$t_1 (\sigma_{xx,1}^0)^2 \left\langle C_3 \frac{E_A^U(\rho_i)}{E_0} \chi_U(\rho_i) \right\rangle \leq \Delta G_m(0 \rightarrow n) \leq t_1 (\sigma_{xx,1}^0)^2 \left\langle C_3 \frac{E_A^L(\rho_i)}{E_0} \chi_L(\rho_i) \right\rangle \quad (82)$$

For evaluation of the *practical* energy release rate bounds for formation of a single microcrack in the middle of an existing microcrack interval of aspect ratio ρ , substitution into (38) leads to

$$\Delta G_{m2}(n \rightarrow n+1) = C_3 t_1 (\sigma_{xx,1}^0)^2 \left(2 \frac{E_A^U(\rho/2)}{E_0} \chi_U(\rho/2) - \frac{E_A^U(\rho)}{E_0} \chi_U(\rho) \right) \quad (83)$$

This result is similar to the previous energy release rate result derived using an assumed strain state [34]. It differs, however, by factors $E_A^U(\rho)/E_0$ because this current analysis is for fixed-displacement boundary conditions while the analysis in Ref. 34 found energy release rate by substituting the effective modulus into a finite energy release rate expression for fixed-load boundary conditions [6, 34].

3.6.3. Sample microcracking calculations

A sample plot of the rigorous bounds $\Delta G_m(0 \rightarrow n)$ for a $[0/90_2]_s$ E-glass/epoxy laminate is given in Fig. 8. This plot is the total energy released per unit area as a function of crack density for loading conditions giving unit stress in the 90°plies ($\sigma_{xx,1}^0 = 1$ MPa). The curves labeled displacement control are the bounds derived in this paper and given in (82). The rigorous bounds for load-control experiments are also plotted; these bounds are derived from the results in Ref. 34. The upper and lower bounds are fairly far apart at low crack density, but get closer at high crack density. The displacement-control upper bound drops much more rapidly than the load-control upper bound. The displacement control bounds get fairly close for crack densities greater than the about 1 mm^{-1} .

The more commonly required energy release rate for analyzing microcracking experiments [2] is the energy release rate for the formation of the next microcrack: $\Delta G_m(n \rightarrow n+1)$. Figure 9 gives a sample calculation of $\Delta G_m(n \rightarrow n+1)$ for $[0/90_2]_s$ E-glass/epoxy laminate as a function of crack density for loading conditions

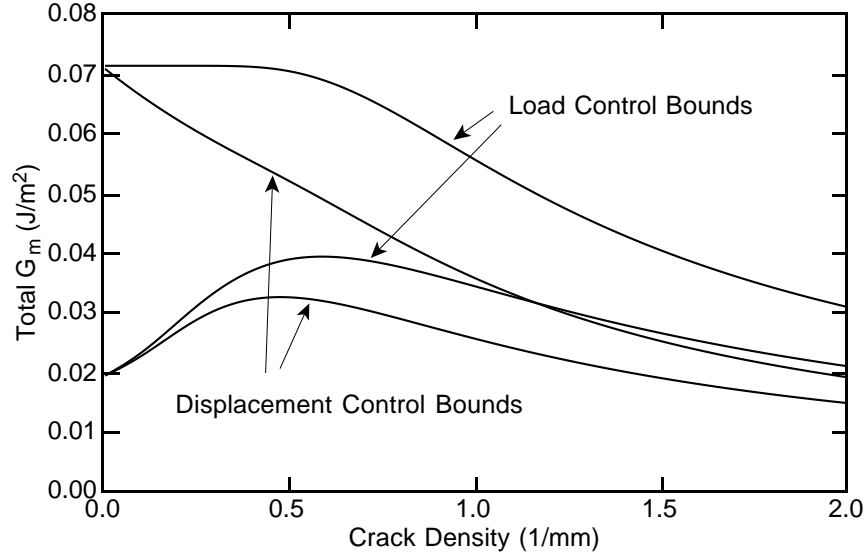


Figure 8. Rigorous bounds on total energy release rate due to formation of all microcracks under displacement control or load control conditions. The calculations are for a $[0/90_2]_s$ E-glass/epoxy laminate. The assumed laminate properties are in Ref. 33. The calculation is for $\sigma_{xx,1}^0 = 1$ MPa.

giving $\sigma_{xx,1}^0 = 1$ MPa. These sample calculations include the rigorous upper and lower bounds (see (36)) and the practical bounds defined in (75) and (83). The symbols give some finite element calculations of the energy release rate. The rigorous upper and lower bounds bound the numerical FEA results but are fairly far apart. The rigorous lower bound becomes negative at high crack density; a tighter lower bound can replace this negative result by the trivial lower bound of zero. The practical bounds (ΔG_{m1} and ΔG_{m2}) always bound the numerical results, but the sense of which practical bound is an upper bound and which is a lower bound switches at a crack density of about 0.6 mm^{-1} . Previous variational mechanics analysis of experimental results have been based on the practical ΔG_{m1} bound [2, 35]. Figure 9 shows that this bound is accurate for all crack densities and very accurate for crack densities greater than about 0.6 mm^{-1} . This improved accuracy at high crack densities may explain, in part, why experimental results typically fit theoretical predictions better at higher crack densities than at lower crack densities [2, 35]. Finally, these practical, displacement-control bounds are tighter to the numerical results than the corresponding practical, load-control bounds plotted in Ref. 34.

4. Conclusions

The key results of this paper are to express global energy analysis of composite fracture in several alternate forms. All of these forms are mathematically identical, but specific forms will be more convenient than other forms for specific composite fracture problems. Equation (7) gives G in terms of mechanical and residual stresses. Equation (12) gives a special case to (7) for mode I crack growth. Equation (18) gives G in terms of initial and perturbation stresses. Equation (14) combines mechanical and residual stresses or initial and perturbation stresses to give G in terms of total stresses. Equations (34) and (36) give variational bounds to ΔG . Each of these results includes residual stresses, traction-loaded cracks, and imperfect interfaces. Most of the equations simplify further when all cracks are traction free and there is no sliding at imperfect interfaces (see, for example, Ref. 6 and (19) and (40)). Even further simplifications are possible when residual stresses are ignored. Because residual stresses are inevitable in composites, however, it is never acceptable to ignore residual stresses. Fortunately, some results in this paper make it possible to account for the effect of residual stresses without ever undertaking thermoelasticity analysis of damaged composites (see (19)).

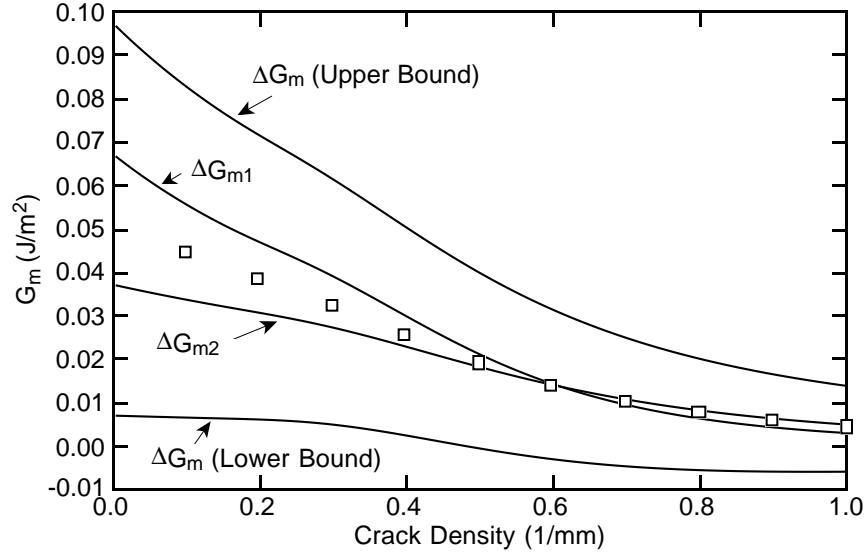


Figure 9. Rigorous (upper and lower bounds) and practical bounds (ΔG_{m1} and ΔG_{m2}) for the energy release rate $\Delta G_m(n \rightarrow n+1)$ or the energy released due to the formation of the next microcrack. The calculations are for a $[0/90_2]_s$ E-glass/epoxy laminate. The assumed laminate properties are in Ref. 33. The calculation is for $\sigma_{xx,1}^0 = 1$ MPa. The symbols are finite element analysis calculations for $\Delta G_m(n \rightarrow n+1)$.

Appendix

A.1. MECHANICAL AND RESIDUAL STRESSES

The energy release rate in (1) requires calculation of internal energy and external work. When the stresses are partitioned into mechanical and residual stresses, the internal energy is:

$$U = \frac{1}{2} \int_V \boldsymbol{\sigma} \cdot (\boldsymbol{\varepsilon} - \boldsymbol{\alpha}T) dV = \frac{1}{2} \int_V \boldsymbol{\sigma}^m \mathbf{S} \boldsymbol{\sigma}^m dV + \int_V \boldsymbol{\sigma}^m \mathbf{S} \boldsymbol{\sigma}^r dV + \frac{1}{2} \int_V \boldsymbol{\sigma}^r \mathbf{S} \boldsymbol{\sigma}^r dV \quad (84)$$

Using the divergence theorem and accounting for all surfaces, the mechanical stress term in (84) may be written in terms of mechanical surface tractions, \vec{T}^m , and displacements, \vec{u}^m , as

$$\frac{1}{2} \int_V \boldsymbol{\sigma}^m \mathbf{S} \boldsymbol{\sigma}^m dV = \frac{1}{2} \int_{S_T} \vec{T}^0 \cdot \vec{u}^m dS + \frac{1}{2} \int_{S_u} \vec{T}^m \cdot \vec{u}^0 dS + \frac{1}{2} \int_{S_c} \vec{T}^m \cdot \vec{u}^m dS \quad (85)$$

The inclusion of the integral over S_c in (85) and in subsequent equations accounts for both traction loaded cracks and imperfect interfaces.

The cross term between mechanical and residual stresses in (84), can be analyzed two separate ways by two applications of virtual work. First, the displacements caused by the residual thermal stresses can be considered as virtual displacements to the mechanical strains. By virtual work including surfaces S_c :

$$\int_V \boldsymbol{\sigma}^m \cdot \boldsymbol{\varepsilon}^r dV = \int_{S_T} \vec{T}^0 \cdot \vec{u}^r dS + \int_{S_c} \vec{T}^m \cdot \vec{u}^r dS \quad (86)$$

Substituting, $\boldsymbol{\varepsilon}^r = \mathbf{S} \boldsymbol{\sigma}^r + \boldsymbol{\alpha}T$ gives:

$$\int_V \boldsymbol{\sigma}^m \mathbf{S} \boldsymbol{\sigma}^r dV = \int_{S_T} \vec{T}^0 \cdot \vec{u}^r dS + \int_{S_c} \vec{T}^m \cdot \vec{u}^r dS - \int_V \boldsymbol{\sigma}^m \cdot \boldsymbol{\alpha}T dV \quad (87)$$

Second, the residual tractions, \vec{T}^r , can be considered as virtual forces on the mechanical stresses. Thus, again by virtual work including surfaces S_c :

$$\int_V \boldsymbol{\varepsilon}^m \cdot \boldsymbol{\sigma}^r dV = \int_V \boldsymbol{\sigma}^m \mathbf{S} \boldsymbol{\sigma}^r dV = \int_{S_u} \vec{T}^r \cdot \vec{u}^0 dS + \int_{S_c} \vec{T}^r \cdot \vec{u}^m dS \quad (88)$$

The residual stress term in (84) can be written as

$$\frac{1}{2} \int_V \boldsymbol{\sigma}^r \mathbf{S} \boldsymbol{\sigma}^r dV = \frac{1}{2} \int_V (\boldsymbol{\sigma}^r \cdot \boldsymbol{\varepsilon}^r - \boldsymbol{\sigma}^r \cdot \boldsymbol{\alpha} T) dV = \frac{1}{2} \left(\int_S \vec{T}^r \cdot \vec{u}^r dS - \int_V \boldsymbol{\sigma}^r \cdot \boldsymbol{\alpha} T dV \right) \quad (89)$$

where S includes all boundary, crack, and interface surfaces. Only the crack and interface surfaces give a non-zero contribution to the surface integral. Thus:

$$\frac{1}{2} \int_V \boldsymbol{\sigma}^r \mathbf{S} \boldsymbol{\sigma}^r dV = \frac{1}{2} \int_{S_c} \vec{T}^r \cdot \vec{u}^r dS - \frac{1}{2} \int_V \boldsymbol{\sigma}^r \cdot \boldsymbol{\alpha} T dV \quad (90)$$

The total external work needs to consider both mechanical and residual displacements on the boundary and both mechanical and residual displacements and tractions on the cracks and interfaces. The work can be written as

$$W = \int_{S_T} \vec{T}^0 \cdot (\vec{u}^m + \vec{u}^r) dS + \int_{S_c} (\vec{T}^m + \vec{T}^r) \cdot (\vec{u}^m + \vec{u}^r) dS \quad (91)$$

Combining (85), (87), (90), and (91) to get potential energy and substitution in (1) leads to the energy release rate theorem given in (7).

A.2 INITIAL AND PERTURBATION STRESSES

When the stresses are partitioned into initial and perturbation stresses, the internal energy can be expressed as:

$$U = \frac{1}{2} \int_V \boldsymbol{\sigma} \cdot (\boldsymbol{\varepsilon} - \boldsymbol{\alpha} T) dV = \frac{1}{2} \int_V \boldsymbol{\sigma}^0 \mathbf{S} \boldsymbol{\sigma}^0 dV + \int_V \boldsymbol{\sigma}^0 \mathbf{S} \boldsymbol{\sigma}^p dV + \frac{1}{2} \int_V \boldsymbol{\sigma}^p \mathbf{S} \boldsymbol{\sigma}^p dV \quad (92)$$

The cross term between initial and perturbation stresses in (92), can be analyzed two separate ways by two applications of virtual work. First, the displacements caused by the perturbation stresses can be considered as virtual displacements to the initial strains. By virtual work accounting for the thermal strains in the initial stresses and including surfaces S_c :

$$\int_V \mathbf{C}(\boldsymbol{\varepsilon}^0 - \boldsymbol{\alpha} T) \cdot \boldsymbol{\varepsilon}^p dV = \int_V \boldsymbol{\sigma}^0 \mathbf{S} \boldsymbol{\sigma}^p dV = \int_{S_T} \vec{T}^0 \cdot \vec{u}^p dS + \int_{S_c} \vec{T}_c^0 \cdot \vec{u}^p dS \quad (93)$$

Second, the perturbation tractions, \vec{T}^p , can be considered as virtual forces on the initial stresses. Thus, again by virtual work including surfaces S_c :

$$\int_V \boldsymbol{\varepsilon}^0 \cdot \boldsymbol{\sigma}^p dV = \int_{S_u} \vec{T}^p \cdot \vec{u}^0 dS + \int_{S_c} \vec{T}^p \cdot \vec{u}^0 dS \quad (94)$$

Substituting $\boldsymbol{\varepsilon}^0 = \mathbf{S} \boldsymbol{\sigma}^0 + \boldsymbol{\alpha} T$ into the first integral leads to

$$\int_V \boldsymbol{\sigma}^0 \mathbf{S} \boldsymbol{\sigma}^p dV = \int_{S_u} \vec{T}^p \cdot \vec{u}^0 dS + \int_{S_c} \vec{T}^p \cdot \vec{u}^0 dS - \int_V \boldsymbol{\sigma}^p \cdot \boldsymbol{\alpha} T dV \quad (95)$$

The perturbation stress term in (92) can be written, using the divergence theorem, as a surface integral

$$\frac{1}{2} \int_V \boldsymbol{\sigma}^p \mathbf{S} \boldsymbol{\sigma}^p dV = \frac{1}{2} \int_S \vec{T}^p \cdot \vec{u}^p dS = \frac{1}{2} \int_{S_c} \vec{T}^p \cdot \vec{u}^p dS \quad (96)$$

As in the residual stress term (see (90)), only the crack and interface surfaces give a non-zero contribution to the surface integral.

The total external work needs to consider both initial and perturbation displacements on the boundary and both initial and perturbation tractions on the cracks and interfaces. The work reduces to

$$W = \int_{S_T} \vec{T}^0 \cdot (\vec{u}^0 + \vec{u}^p) dS + \int_{S_c} \vec{T}_c \cdot (\vec{u}^0 + \vec{u}^p) dS \quad (97)$$

Combining (92), (93), (96), and (97), the potential energy can be written as

$$\Pi = \Pi_0 - \int_{S_c} \vec{T}^p \cdot \vec{u}^0 dS - \frac{1}{2} \int_{S_c} \vec{T}^p \cdot \vec{u}^p dS \quad (98)$$

where

$$\Pi_0 = \frac{1}{2} \int_V \boldsymbol{\sigma}^0 \mathbf{S} \boldsymbol{\sigma}^0 dV - \int_{S_T} \vec{T}^0 \cdot \vec{u}^0 dS - \int_{S_c} \vec{T}_c^0 \cdot \vec{u}^0 dS \quad (99)$$

is the potential energy of the initial stress state. Substitution of (98) into (1) and use of (96) and Hooke's law for the perturbation stresses leads to the results in (18).

Acknowledgments

This work was supported, in part, by a grant from the Mechanics of Materials program at the National Science Foundation (CMS-9713356), and, in part, by the University of Utah Center for the Simulation of Accidental Fires and Explosions (C-SAFE), funded by the Department of Energy, Lawrence Livermore National Laboratory, under Subcontract B341493.

References

1. S. Hashemi, A. J. Kinloch, and J. G. Williams (1990). The Analysis of Interlaminar Fracture in Uniaxial Fibre Reinforced Polymer Composites. *Proceedings of the Royal Society of London* **A347**, 173–199.
2. J. A. Nairn and S. Hu (1994). Micromechanics of Damage: A Case Study of Matrix Microcracking. In: *Damage Mechanics of Composite Materials* (edited by R. Talreja), Elsevier, Amsterdam, 187–243.
3. W. M. Jordan and W. L. Bradley (1987). Micromechanisms of Fracture in Toughened Graphite-Epoxy Laminates. In: *Toughened Composites* (edited by N. J. Johnston), ASTM STP **937**, 95–114.
4. J. G. Williams (1984). *Fracture Mechanics of Solids*, John Wiley & Sons, New York.
5. J. A. Nairn and P. Zoller (1985). Matrix Solidification and the Resulting Residual Thermal Stresses in Composites. *Journal of Material Science* **20**, 355–367.
6. J. A. Nairn (1997). Fracture Mechanics of Composites With Residual Thermal Stresses. *Journal of Applied Mechanics* **64**, 804–810.
7. Z. Hashin (1990). Thermoelastic Properties of Fiber Composites With Imperfect Interface. *Mechanics of Materials* **8**, 333–348.
8. Z. Hashin (1996). Finite Thermoelastic Fracture Criterion with Application to Laminate Cracking Analysis. *Journal of the Mechanics and Physics of Solids* **44**, 1129–1145.
9. B. W. Rosen and Z. Hashin (1970). Effective Thermal Expansion Coefficients and Specific Heats of Composite Materials. *International Journal of Engineering Science* **8**, 157–173.
10. R. A. Schapery (1968). Thermal Expansion Coefficients of Composite Materials Based on Energy Principles. *Journal of Composite Materials* **3**, 380–403.
11. L. N. McCartney (1998). Prediction of Microcracking in Composite Materials. In *Fracture: A Topical Encyclopedia of Current Knowledge Dedicated to Alan Arnold Griffith*, (editid by G. P. Cherepanov), Krieger Publishing Company, Melbourne, USA.
12. V. M. Levin (1967). On the Coefficients of Thermal Expansion in Heterogeneous Materials. *Mechanics of Solids* **2**, 58–61.
13. D. E. Carlson (1984). Linear Thermoelasticity. In: *Mechanics of Solids, Volume II* (edited by C. Truesdell), Springer-Verlag, New York, 297–345.
14. Z. Hashin (1985). Analysis of Cracked Laminates: A Variational Approach. *Mechanics of Materials* **4**, 121–136.
15. L. T. Drzal, Rich, M. J. and Lloyd, P. F. (1983a). Adhesion of Graphite Fibers to Epoxy Matrices: I. The Role of Fiber Surface Treatment. *Journal of Adhesion* **16**, 1–30.
16. T. K. O'Brien (1985). Analysis of Local Delaminations and Their Influence on Composite Behavior. In: *Delamination and Debonding of Materials* (edited by W. S. Johnson), ASTM STP **876**, 282–297.

17. J. A. Nairn and Y. C. Liu (1997). On the Use of Energy Methods for Interpretation of Results of Single-Fiber Fragmentation Experiments. *Composite Interfaces* **4**, 241–267.
18. J. A. Nairn and S. R. Kim (1992). A Fracture Mechanics Analysis of Multiple Cracking in Coatings. *Engineering Fracture Mechanics* **42**, 195–208.
19. S. R. Kim and J. A. Nairn (2000). Fracture Mechanics Analysis of Coating/Substrate Systems Subjected to Tension or Bending Loads I: Theory. *Engineering Fracture Mechanics*, in press.
20. S. R. Kim and J. A. Nairn (2000). Fracture Mechanics Analysis of Coating/Substrate Systems Subjected to Tension or Bending Loads II: Experiments in Bending. *Engineering Fracture Mechanics*, in press.
21. C. H. Liu and J. A. Nairn (2000). Analytical Fracture Mechanics of the Microbond Test Including the Effects of Friction and Thermal Stresses. *Journal of Adhesion and Adhesives* **19**, 59–70.
22. E. F. Rybicki and M. F. Kanninen (1977). A Finite Element Calculation of Stress Intensity Factors By a Modified Crack Closure Integral. *Engineering Fracture Mechanics* **9**, 931–938.
23. J. A. Nairn and Y. C. Liu (1997). Stress Transfer into a Fragmented, Anisotropic Fiber Through an Imperfect Interface. *International Journal of Solids and Structures* **34**, 1255–1281.
24. J. O. Outwater and M. C. Murphy (1970). Fracture Energy of Unidirectional Laminates. *Modern Plastics September Issue*, 160–168.
25. Y. C. Liu (1997). Micromechanics Analysis of the Single Fiber Fragmentation Test to Give a Better Understanding of the Fiber/Matrix Interface in Composite Materials. Ph.D. Thesis, University of Utah.
26. L. N. McCartney (1993). Stress Transfer Mechanics for Multiple Perfectly Bonded Concentric Cylinder Models of Unidirectional Composites. *National Physical Lab Report DMM(A)129*, 1–28.
27. H. D. Wagner, J. A. Nairn, and M. Detassis (1995). Toughness of Interfaces from Initial Fiber-Matrix Debonding in a Single-Fiber Composite Fragmentation Test. *Applied Composite Materials* **2**, 107–117.
28. M. Detassis, E. Frydman, D. Vrieling, X.-F. Zhou, J. A. Nairn, and H. D. Wagner (1996). Interface Toughness in Fiber Composites by the Fragmentation Test. *Composites* **27A**, 769–773.
29. X.-F. Zhou, J. A. Nairn, and H. D. Wagner (1999). Fiber-Matrix Adhesion From the Single-Fiber Composite Test: Nucleation of Interfacial Debonding. *Composites* **30**, 1387–1400.
30. J. A. Nairn and H. D. Wagner (1996). A Revised Shear-Lag Analysis of an Energy Model for Fiber-Matrix Debonding. *Advanced Composite Letters* **5**, 131–135.
31. J. A. Nairn (1997). On the Use of Shear-Lag Methods for Analysis of Stress Transfer in Unidirectional Composites. *Mechanics of Materials* **26**, 63–80.
32. J. A. Nairn (1989). The Strain Energy Release Rate of Composite Microcracking: A Variational Approach. *Journal of Composite Materials* **23**, 1106–1129. (and errata: *Journal of Composite Materials* **24** (1990) 233).
33. J. Varna and L. A. Berglund (1992). A Model for Prediction of the Transverse Cracking Strain in Cross-Ply Laminates. *Journal of Reinforced Plastics and Composites* **11**, 708–728.
34. J. A. Nairn (1995). Some New Variational Mechanics Results on Composite Microcracking. *Proceedings of the 10th International Conference on Composite Materials* **I**, 423–430.
35. J. A. Nairn, S. Hu, and J. S. Bark (1993). A Critical Evaluation of Theories for Predicting Microcracking in Composite Laminates. *Journal of Material Science* **28**, 5099–5111.